

Facies analysis and sequence stratigraphy of an Upper Jurassic carbonate ramp in the Eastern Alborz range and Binalud Mountains, NE Iran

A. Aghaei · A. Mahboubi · R. Moussavi-Harami ·
C. Heubeck · M. Nadjafi

Received: 27 February 2012 / Accepted: 12 October 2012
© Springer-Verlag Berlin Heidelberg 2012

Abstract Upper Jurassic (Oxfordian-Kimmeridgian-Tithonian?) strata of NE Iran (Lar Formation) are composed of medium- to thick-bedded, mostly grainy limestones with various skeletal (bivalves, foraminifera, algae, corals, echinoderms, brachiopods, and radiolaria) and nonskeletal (peloids, ooids, intraclasts, and oncoids) components. Facies analysis documents low- to high-energy environments, including tidal-flat, lagoonal, barrier, and open-marine facies. Because of the wide lateral distribution of facies and the apparent absence of distinct paleobathymetric changes, the depositional system likely represents a westward-deepening homoclinal ramp. Four third-order depositional sequences can be distinguished in each of five stratigraphic measured sections. Transgressive system tracts (TST) show deepening-upward trends, in which shallow-water (tidal flat and lagoonal) facies are overlain by deeper-water (barrier and open-marine) facies. Highstand systems tracts (HST) show shallowing-upward trends in which deep-water facies are overlain by shallow-water facies. All sequence boundaries in the study area (except at the top of the stratigraphic column) are of the nonerosional (SB2) type. Correlation of depositional sequences in the studied sections show that relatively shallow marine (tidal-flat, lagoonal, barrier, and shallow open-marine) conditions dominated in the area. These alternated with deep-water open-marine wackestone and mudstones representing zones of maximum flooding (MFZ).

Keywords Upper Jurassic · Lar Formation · Northeast Iran · Alborz · Binalud · Facies analysis · Sequence stratigraphy · Carbonate ramp

Introduction

Present-day Iran is part of the Alpine-Himalayan orogenic belt, which is bordered by the Arabian Shield to the southwest and the Turan Plate to the northeast (Fig. 1). However, a large part of Iran, consisting of the Central-East Iranian Microcontinent, northwest Iran, and the Alborz Mountains form the composite Iranian Plate (Fig. 2), part of the former Cimmerian microcontinent, which rifted from the northern margin of Gondwana in the Early Permian. North of Cimmeria, the Paleo-Tethys Ocean was subducted along an active plate margin extending at least from Greece to the Himalayas along the southern margin of Eurasia; south of Cimmeria, the Mesozoic Neotethys opened between Gondwana and Cimmeria (Sengör 1979, 1990; Stampfli et al. 1991; Stampfli and Borel 2002; Seyed-Emami 2003; Moix et al. 2008; Fürsich et al. 2009; Wilmsen et al. 2010; Ghasemi-Nejad et al. 2012; and many others).

Cimmeria, including the composite Iran Plate, collided with the southern margin of Eurasia (the Turan Plate) in the Late Triassic—Early Jurassic, closing the Paleo-Tethys. In Iran, this suture is believed to lie within the Alborz, Kopet Dag and Binalud Mountains (Alavi 1992; Alavi et al. 1997; Zanchi et al. 2006; Ramezani Oomali et al. 2008) and the closing is marked by the formation of a southward-facing, Norian to Aalenian, terrestrial-facies foreland basin in central Iran (the Shemshak Group; Davoudzadeh and Schmidt 1981; Wilmsen et al. 2009a, b; Moosavirad et al. 2011). In northern Iran and along tectonic strike to the east and the west, remnants of the Paleo-Tethys continued to

A. Aghaei · A. Mahboubi · R. Moussavi-Harami · M. Nadjafi
Department of Geology, Ferdowsi University of Mashhad,
Mashhad, Iran

C. Heubeck (✉)
Department of Geological Sciences, Freie Universität Berlin,
Berlin, Germany
e-mail: christoph.heubeck@fu-berlin.de

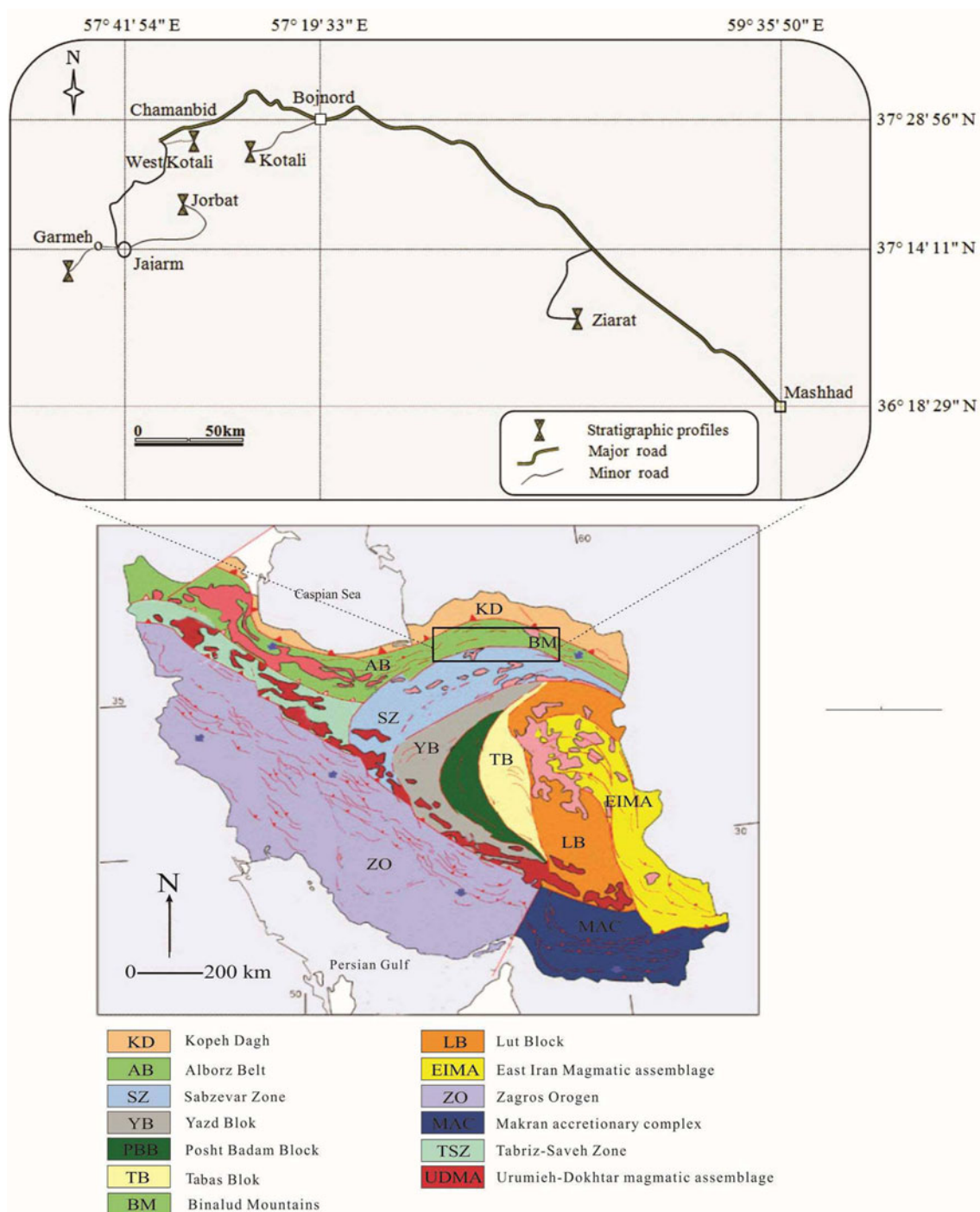
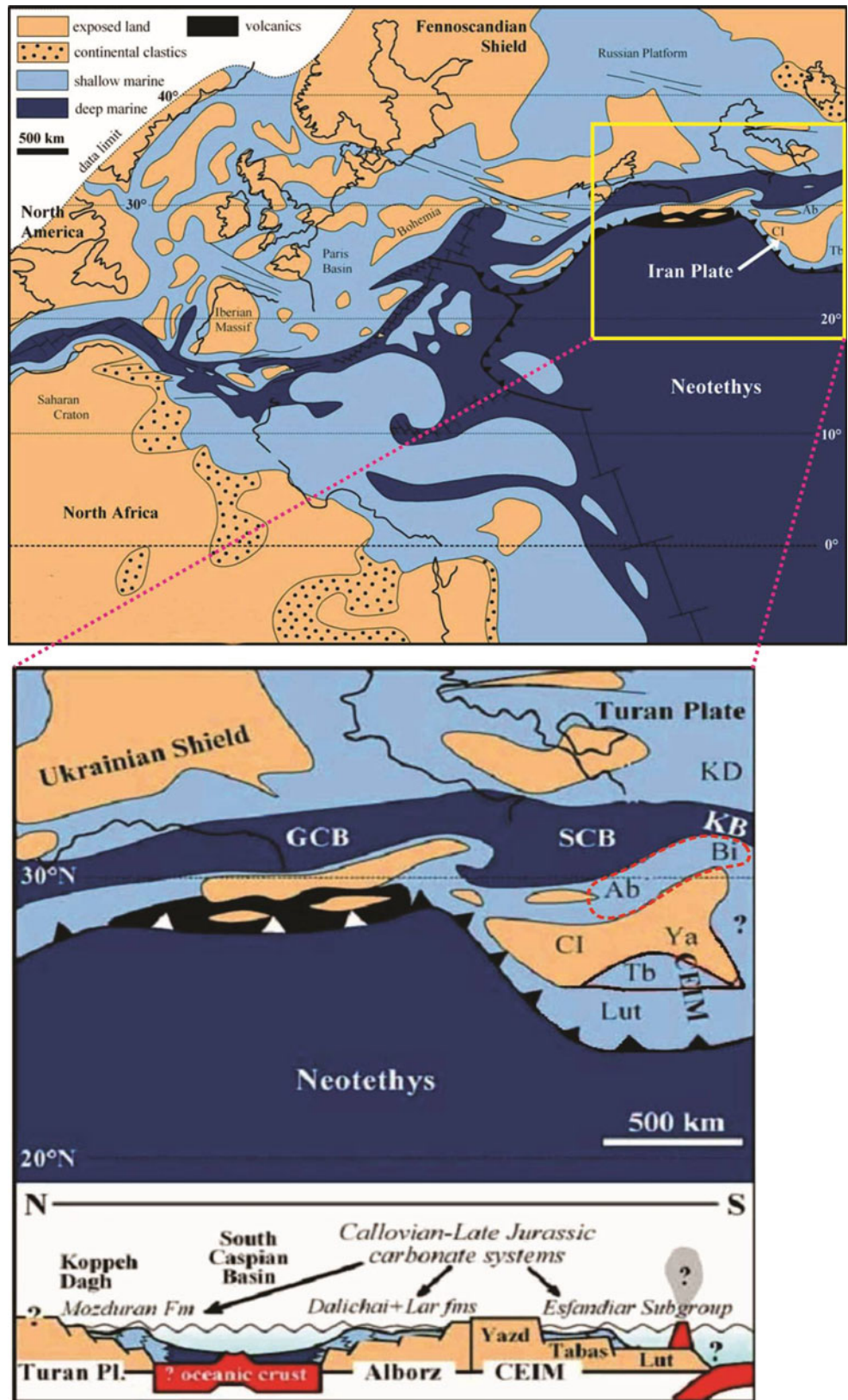


Fig. 1 Location map of the study area (modified after Alavi 1991) showing locations of measured stratigraphic sections

exist in small remnant ocean basins and in newly formed Jurassic back-arc marginal basins between the former Cimmerian and Eurasian terranes along the southern margin of the East Pontides, Transcaucasus, Talysh and Alborz plates (Zonenshain and Le Pichon 1986; Sengör 1990; Brunet et al. 2003a, b); Golonka (2004) named this elongate basin the Greater Caucasus—Proto-Caspian back-arc

basin. Marine sedimentation began in the Late Bajocian and Bathonian when the Northern Alborz, Kopet–Dagh, and Central Iran basins formed on the Iranian Plate. Initial siliciclastic deposits were followed in the Middle Jurassic by marly carbonates (the Dalichai Formation), possibly reflecting lower rates of subsidence (Fürsich et al. 2009). The growing deposition of carbonates was also facilitated

Fig. 2 Paleogeographic and tectonic setting of the Callovian-Late Jurassic carbonate systems of northern Iran (modified after Wilmsen et al. 2009a, b). *Tb* Tabas, *Ya* Yazd Blocks, *Ab* Alborz, *Bi* Binalud Mountains, *CI* Central Iran, *GCB* Greater Caucasus Basin, *KB* Kashafrud Basin, *KD* Kopet Dagh, *SCB* South Caspian Basin. *Lut* Lut Block; *CEIM* Central-East Iranian Microcontinent. *Dashed red line* shows location of study area in the Binalud and Alborz Mountains of northern Iran



by southward migration of the Iranian plate, which had occupied a fairly high latitudinal position of approximately N 44° during the Early Jurassic (Dercourt et al. 2000), to a

lower latitude of ca. 20–30°N during the Middle Callovian (Thierry 2000; Seyed-Emami et al. 2008; Wilmsen et al. 2010; Ghasemi-Nejad et al. 2012). Middle Jurassic

ammonite faunas of the Central Alborz basin show close similarities to those from neighboring subbasins as well as to those of European and Mediterranean regions (Shams 2007; Seyed-Emami et al. 2008; Ghasemi-Nejad et al. 2012). Thus, architecture, facies and thickness of widespread Late Jurassic strata in northern Iran reflect continued tectonic instability within a low-latitude back-arc setting on continental crust.

This study integrates the findings from five key stratigraphic sections of the Late Jurassic Lar Formation, a marine carbonate platform in the eastern Alborz and Binalud Mountains and part of the northern margin of the Iran Plate. The strata of the Lar Formation form structurally part of the Alborz belt, a ~1,500-km-long mountain range extending from Azerbaijan to Afghanistan that formed due to the Eo-Cimmerian orogeny (Early Permian) and due to Tertiary–Quaternary intracontinental transpression (Allen et al. 2003), and to the adjacent Binalud Mountains, an east–west-trending sinusoidal ridge in northeast Iran which formed due to Cenozoic folding (Alavi 1991; Shabanian et al. 2010). Both ranges are still seismically very active (Ritz et al. 2006; e.g., Majidifard 2008; Wilmsen et al. 2010; Seyed-Emami and Schairer 2011; Figs. 1, 2).

Strata of the Lar Formation, which formed extensive basinal and platform carbonate environments, overlie Middle Jurassic marls of the Dalichai Formation and underlie Cretaceous siliciclastic strata (Fig. 3). Base and top of the Dalichai and Lar formations are diachronous, probably due to tectonic processes in the back-arc (Lasemi 1995; Majidifard 2008). In the studied sections, their stratigraphic age is Oxfordian–Kimmeridgian, based on foraminifers (Aghaei et al. 2012). Carbonates of the Lar Formation are ~220 to ~530 m thick and are erosionally truncated by terrestrial sandstones and conglomerates of Early Cretaceous age (Fig. 3). They are principally composed of thin-bedded (10–30 cm), grey to tan and light brown limestones with common chert nodules in the lower part, overlain by medium- to thick-bedded (0.5–2 m) and massive, grey limestones with less chert nodules in the upper part. The depositional environment ranged from tidal-flat to open-marine (Mahboubi et al. 2006, 2010; Fig. 4). Fossils include ammonites, bivalves, echinoderms, rare belemnites, radiolarians, sponge spicules, and benthic foraminifers. The Dalichai and Lar formations closely resemble the Pınarbaşı successions of Turkey (Demirtaslı 1984a, b), recording the opening of the Paleo- and Neotethys (Moix et al. 2008).

The objectives of this contribution are to reconstruct depositional environments of the Late Jurassic back-arc environment of Northern Iran, to constrain its controlling tectonic and climatic factors, and to improve the understanding of the Jurassic tectonics and palaeogeography of central Asia.

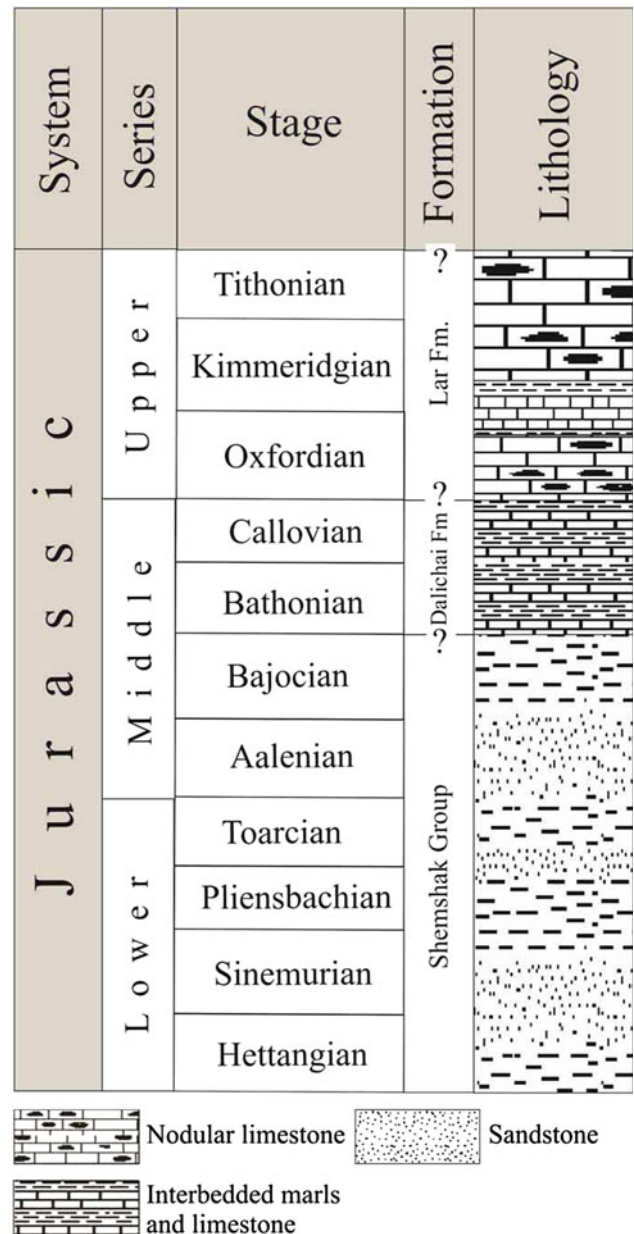


Fig. 3 Lower to Upper Jurassic lithostratigraphic units in the eastern Alborz Mountains (modified from Fürsich et al. 2005)

Methods

Five stratigraphic sections were measured and sampled with an emphasis on lithology and the characterization of sedimentary structures. Detailed petrographic studies were based on approximately 700 thin-sections (Fig. 1) stained with Alizarin Red S and potassium ferricyanide solution (Dickson 1966). Carbonate rocks were classified following Dunham (1962), Folk (1962), and Embry and Klovan (1971). In addition, clasticity indices were measured for ooid, intraclast and echinoderm fragments in some facies, following Carozzi (1993).

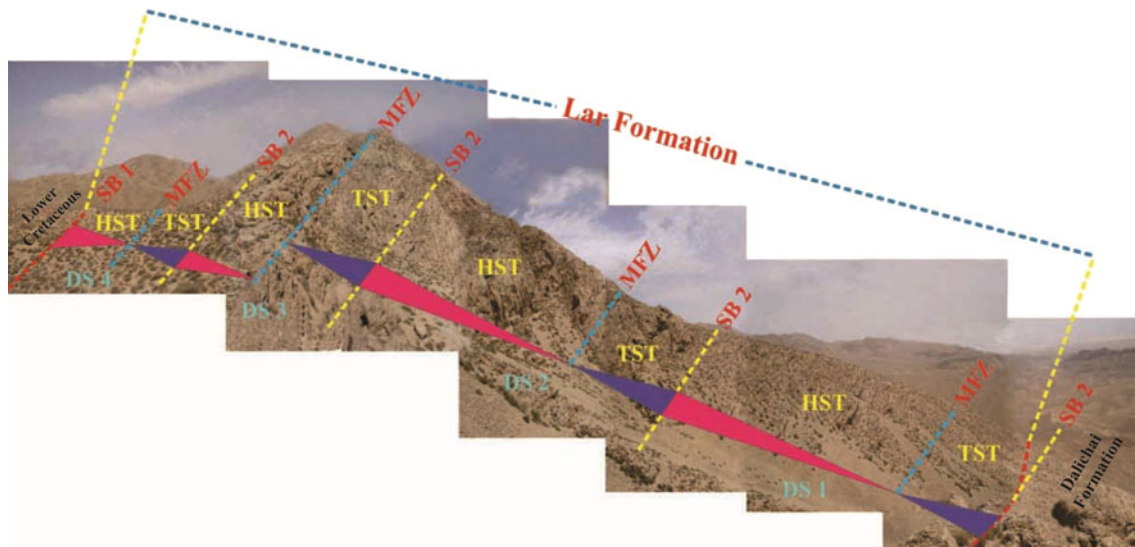


Fig. 4 Characteristic outcrop of Upper Jurassic carbonates in the study area (Garmeh section) overlain by Cretaceous siliciclastic strata

Depositional sequences and inferred relative sea level changes were interpreted based on the Carrozi method (Carozzi 1993). Facies identification and stacking patterns of facies followed the classification of Schlager (2005) and Catuneanu et al. (2009). Depositional sequence-stratigraphic tracts were defined based on facies trends, stacking pattern, lithological changes, and named following Van Wagoner et al. (1988, 1990). These sequence-stratigraphic tracts were then correlated with each other based on facies and depositional environments and finally related to the global sea level curves of Haq et al. (1988).

Results

Facies associations

On the basis of detailed facies analysis, the vertical and lateral distribution of the facies types, the lack of distinct bathymetric changes (Wright and Burchette 1998) and the comparison with similar facies (e.g., Brachert et al. 2001; Corda and Brandano 2003; Mahboubi et al. 2010; Bassi and Nebelsick 2010; Van Buchem et al. 2010), we propose a ramp model for the carbonate deposits in the study area.

Based on lithology, sedimentary structures, textures, and the presence and proportion of skeletal (mainly bivalves, corals, calcareous sponges, gastropods, and echinoids) and nonskeletal (peloid, ooid, intraclast and oncoid) grains, the depositional environment of the studied strata is marine and includes tidal-flat (T1–T3), lagoonal (L1–L7), barrier (B1–B7), and open-marine (O1–O8) facies. These are described and interpreted basinward as below:

Tidal flat

Two carbonate (T1 and T2) and one marly (T3) facies are identified in this depositional environment. They are buff to light grey and thin- to thick-bedded (0.3–2 m).

Unfossiliferous Lime Mudstone (T1): Facies T1 consists of very thin, medium- to thick-bedded, mostly nonlaminated and homogeneous lime mudstones, occasionally marly limestones. Lime mudstones contain only scattered skeletal grains (bivalves) and scattered silt and sand-sized quartz grains, in places showing fenestral fabric (Fig. 5a).

Dolomudstone (T2): Facies T2 consists of tan to light grey, thick-bedded (about 1–2 m), very finely crystalline, homogeneous but in places laminated, nonferroan dolomite (Fig. 5b). In places, the dolomite diagenetically recrystallized to coarser crystals.

Marl (T3): Marly intervals vary in thickness from a few centimeters to several meters and occur especially at the base and near the top of the succession (Fig. 5c). Marls are light grey to grey, thin-bedded (<0.1–0.2 m), rarely laminated, and low in fossils, which consist of a poor and little diversified fauna of thin-shelled bivalves and foraminifera.

Interpretation The unfossiliferous mudstones and dolomudstones (T1, T2) correspond to facies SMF-23 of Wilson (1975) and Flügel (2010). The fine grain size, the presence of quartz grains, the lack of fauna, the fenestral fabric and vertical changes suggest that deposition occurred in a low-energy, restricted intertidal and supratidal environment (e.g., Wilson and Evans 2002; Amirshahkarami et al. 2007; Wilmsen et al. 2010). Marls (T3) are interpreted as having been deposited on tidal flats because they contain a low-diversity shallow-water biota, a low



Fig. 5 Tidal-flat facies. **a** Unfossiliferous mudstone with scattered silt- to sand-sized quartz grains, Ziarat section (T1); thin-section. **b** Dolomudstone, Kotali section (T2); thin-section. **c** Marl beds, west Kotali section (T3). *Compass* for scale

proportion of bivalve fragments, and a few foraminifera (e.g., Rush and Kerans 2010).

Lagoon

Lagoonal facies in general are characterized by a large proportion of mud and the presence of abundant benthic foraminifera, gastropods, and bivalves (Husinec and Sokac 2006; Bachmann and Hirsch 2006; Palma et al. 2007; Adabi et al. 2010; Flügel 2010). In the study area, these include seven facies (L1–L7).

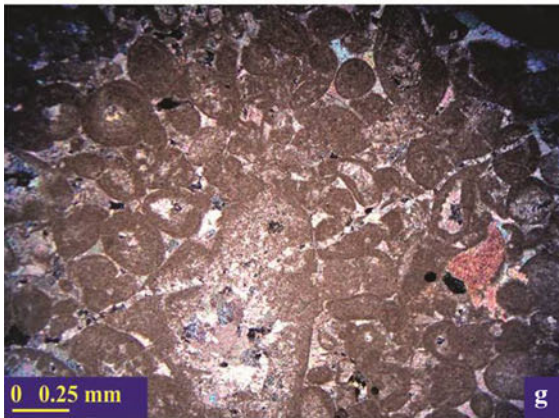
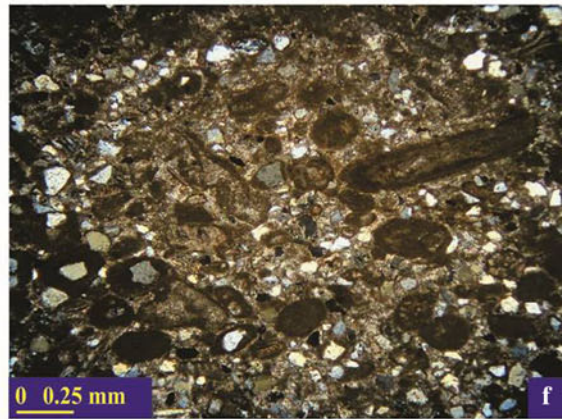
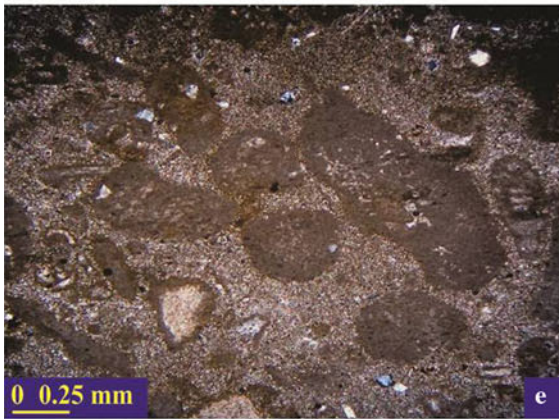
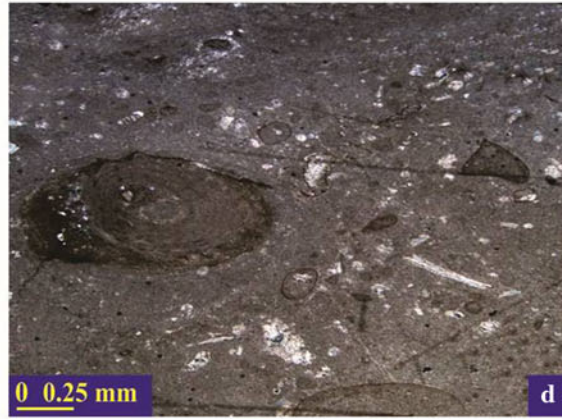
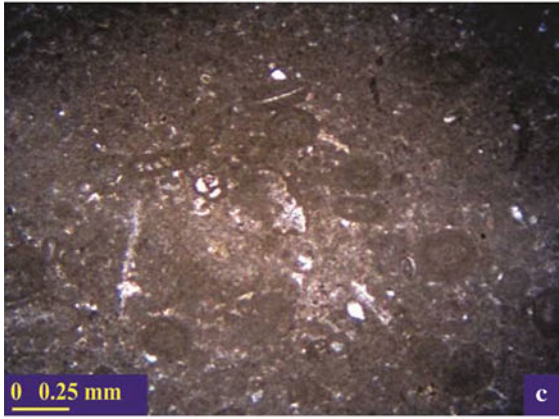
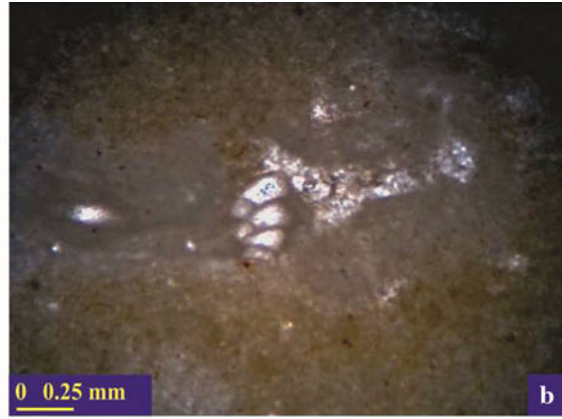
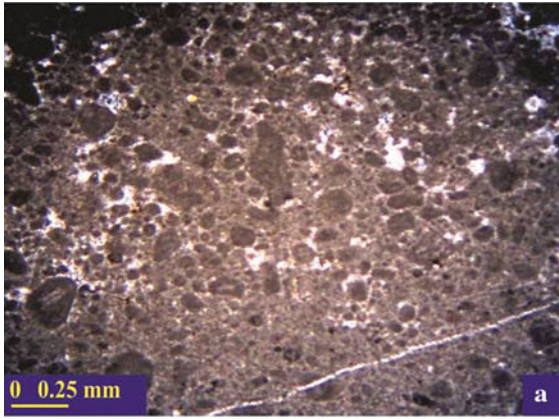
Peloid wackestone/packstone (L1): This facies is widespread in the study area. Peloids are dominant and constitute from 10 to 80 % of the carbonate grains in thin-section. The size of peloids ranges between 0.1 and 0.5 mm (Fig. 6a). Peloids are spherical, ellipsoidal or angular but are mostly well rounded and show weak to moderate sorting. In some beds, they form a densely packed, grain-supported fabric. Other grains include bivalve fragments (2–3 %) and foraminifera (1–2 %).

Fig. 6 Thin-sections of lagoonal facies. **a** Peloid wackestone/packstone, Ziarat section (L1). **b** Foraminifera mudstone, Ziarat section (L2). **c** Foraminifera-peloid wackestone/packstone, Jorbat section (L3). **d** Peloid-oncoid wackestone, Kotali section (L4). **e** Intraclast wackestone, west Kotali section (L5). **f** Sandy peloid-oid wackestone, Ziarat section (L6). **g** Ooid-peloid packstone/grainstone, Kotali section (L7)

Bioclastic mudstone (L2): This facies includes miliolids and textulariids with scattered peloids (Fig. 6b). The rocks are medium- to thick-bedded (0.2–1 m), in places laminated, and grey to buff-colored.

Foraminifera-peloid wackestone/packstones (L3): The proportion of foraminifera ranges from 15 to 50 % and includes miliolids and textulariids (Fig. 6c). Bivalve (1–2 %) and peloids (about 5 %) are present. Peloids often merge to a pseudo-micritic matrix, causing a clotted texture. There are also very low proportions of scattered ooids and oncoids in this facies.

Peloid-oncoid wackestone (L4): L4 is characterized by a mud-dominated fabric and the presence of oncoid and



benthic foraminifera. Oncoids vary from 1 to >2 mm; concentric C-oncoids are rare (e.g., Adachi et al. 2004). Bioclast nuclei make up ~20 %. Other grains such as peloids (~10 %) and bioclasts consisting of foraminifera and small proportions of bivalves (~6–7 %) are present (Fig. 6d). These limestones are fine-grained, grey to tan colored, medium- to thick-bedded (0.2–2 m) but in places laminated.

Intraclast wackestone (L5): L5 is composed of intraclasts (~25 %) ranging in size from ~0.5 to 2 mm displaying relatively smooth and subangular edges, fine-grained silt- to sand-sized quartz grains (~3 %), and very low proportions of miliolids and bivalve fragments (~1–2 %) (Fig. 6e). They appear as medium-grained (1–2 mm) grey to tan calcarenites in the field.

Sandy peloid-oid wackestone (L6): Ooids (15 %), peloids (10 %) and intraclasts (5 %) are the principal grains in this facies. Fine- to medium-size quartz grains are present (15 %). Bioclasts are very low (~2 %) in proportion and consist of miliolids, gastropods, echinoderms (Fig. 6f). Ooids are in places affected by micritization; where this is the case, their microfabric is mostly destroyed. Gastropod, bryozoan and bivalve fragments are also observed in hand samples. They are light brown without any distinct sedimentary structures in the field.

Ooid-peloid packstone/grainstone (L7): Peloids (50–60 %), ooids (10–12 %), bioclasts (bivalve and low proportions of coral and echinoderms; ~2 %) and intraclasts (1–2 %) are present (Fig. 6g). Ooids are in place affected by micritization. In the field, this rock type appears fine- to medium-grained (mostly <1 mm), is buff-colored to grey, and thick-bedded (2–3 m) to massive.

Interpretation A semiarid climate and restricted water circulation led to partly hypersaline conditions with a restricted fauna (Flügel 2010). The very common peloidal wacke- to packstones (L1) indicate widespread low-energy, somewhat restricted peritidal environments punctuated only episodically by high-energy events such as storms and spring tides. The textural characteristics and dominance of miliolids, bivalves and in places gastropods, the absence of larger foraminifera, textulariids, algal fragments, open-marine fauna and the presence of some micritized grains and intraclasts suggest a very shallow-marine backshoal environment. It represents a semi-restricted lagoon in close vicinity of tidal flats with relatively low currents (e.g., Geel 2000; Romero et al. 2002; Vaziri-Moghaddam et al. 2006; Badenas and Aurell 2010) where large fluctuations in salinity and temperature may have occurred (Martini et al. 2007). In the fine- to coarse-grained, nonlaminated wackestones/packstones, the low diversity of bioclasts (only foraminifera) and the dominance of peloids in facies L4, L5, L6, and L7 indicate deposition on an inner ramp but

Fig. 7 Thin-sections of barrier facies. **a** Peloid grainstone, Ziarat section (B1). **b** Ooid grainstone, west Kotali section (B2). **c** Intraclast grainstone, Jorbat section (B3). **d** Ooid-intraclast-bioclast grainstone, west Kotali section (B4). **e** Intraclast-peloid packstone/grainstone with bioclast, Kotali section (B5). **f** Peloid-oid grainstone, Jorbat section (B6). **g** Peloid-bioclast-oid grainstone, Garmeh section (B7)

perhaps also in a peritidal setting with a poor connection to a middle ramp (Martini et al. 2007). Grain-support and the low biotic diversity of facies L1, L3, and L7 indicate that these sediments were deposited in protected, restricted, well-oxygenated, low-energy environments (Wilson 1975; Buonocunto et al. 1994; Martini et al. 2007; Flügel 2010). The abundance of micritized grains suggests occasional breaks in sedimentation (Hips and Haas 2009).

Oncoidal limestones (L4) are best related to a back-barrier, shallow, open-lagoonal and (to a minor degree) closed-lagoonal facies (Wilson 1975; Alesi 1984; Aigner 1985; Schauer and Tebingen 1997). A similar facies has also been described, e.g., in the Late Jurassic Plassen carbonate platform of the Northern Calcareous Alps (Austria and Germany) (Schlagintweit and Gawlick 2009). According to Wilson (1975) and Flügel (2010), oncologic wackestones are typical of shallow, relatively quiet back-bank environments where they form at the margins of ponds and channels and where they are subjected to intermittent current activity and relatively low sedimentation rates, indicated by micritic envelopes (Palma et al. 2007; Papaioannou and Kostopoulou 2008; Kavooosi et al. 2009; Brigaud et al. 2010; Wilmsen et al. 2010). A warm, euphotic environment is also supported by the very low proportions of bryozoans, corals, and echinoderms (L6 and L7).

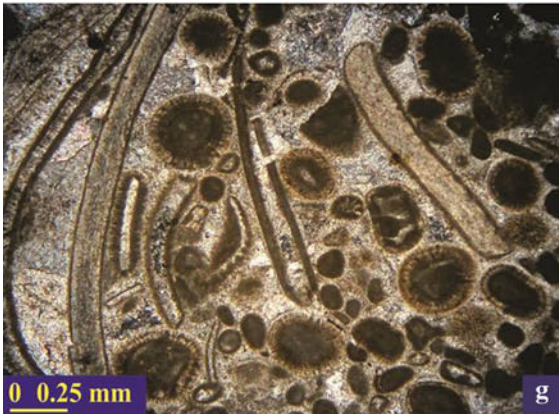
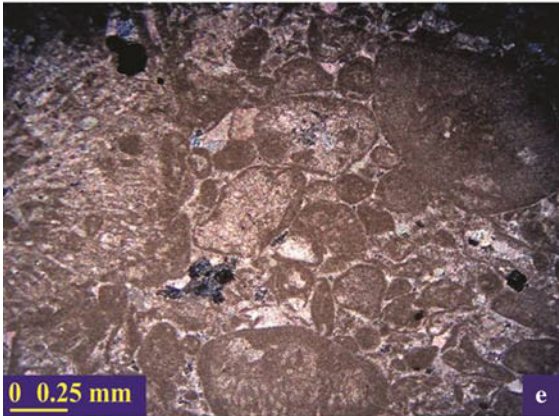
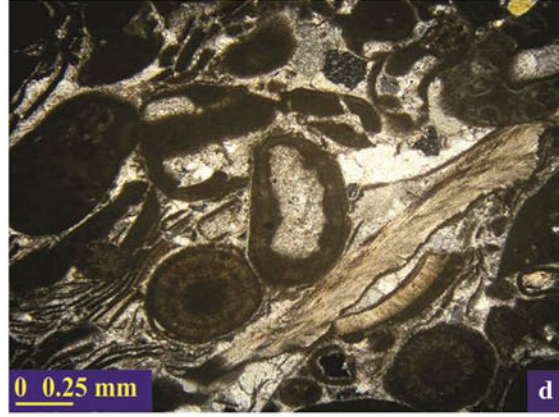
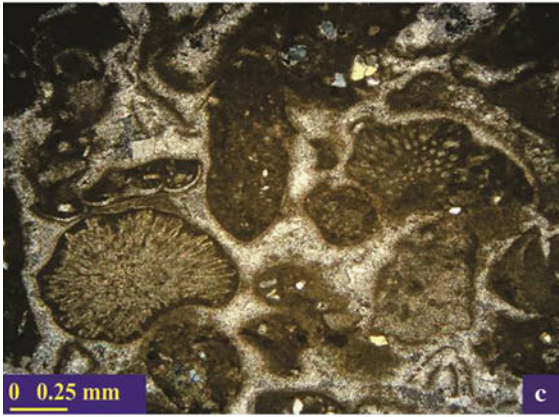
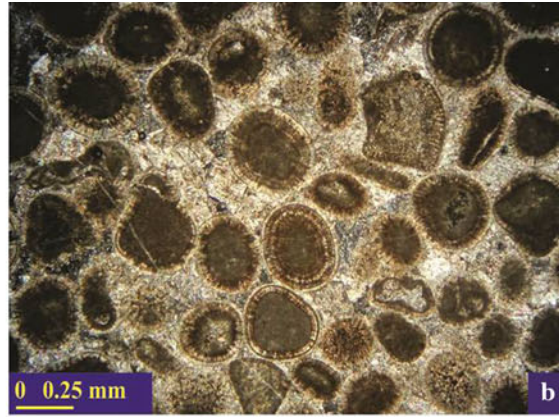
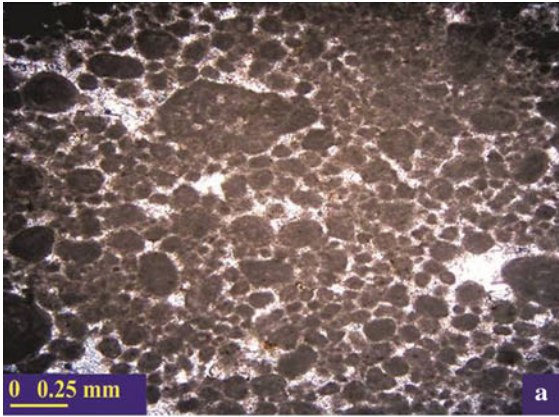
Barrier

Facies B1 to B7 are associated with barrier environments and are mainly composed of grainstones.

Peloid grainstone (B1): Facies B1 is mostly composed of nonskeletal grains (~50 % peloids and ~5 % ooids); a few scattered small-sized intraclasts and bioclasts are also present. Skeletal grains are rare and only consist of bivalve fragments (~1 %) (Fig. 7a). The limestone is fine-grained, grey, thick-bedded (2–3 m) and exhibits cross-lamination.

Ooid packstone-grainstone (B2): The dominant well-sorted radial ooids, 0.5–1.5 mm in size, have in places been replaced by granular, blocky, and drusy sparry calcite cement; some are microbially micritized (Fig. 7b). Nuclei consist of various skeletal and nonskeletal fragments. Scattered aggregate grains are present but rare (<1 %). In outcrop, B2 is a thick-bedded (0.5–1 m), in places cross-bedded, grey calcarenite with marly interbeds.

Intraclast grainstone (B3): This facies consists of well-rounded but poorly sorted intraclasts (~50 %), gastropods,



echinoderms, and bryozoan bioclasts (total ~7–8 %) (Fig. 7c). Granular and blocky sparry calcite fills the interstices between grains. In the outcrop, beds consist of coarse-grained, buff-colored, thick-bedded (2–3 m) and cross-bedded calcarenite to calcirudite.

Ooid-intra-bioclast grainstone (B4): Bioclasts (40 %) in this facies include bivalve (25 %), brachiopod (10 %), echinoderm (5 %), and gastropod (1 %) fragments ranging in size from millimeters to several centimeters. Intraclasts (15 %) and ooids (10 %) represent the dominant nonskeletal grains (Fig. 7d). Ooid size ranges from 0.6 to 1.2 mm; intraclasts are <1 to ~2 mm in diameter. Micritization has destroyed the internal microfabric of some ooids and bioclasts. Micritic envelopes are not pervasive but can be observed on some grains. In the field, the beds appear as dark grey, thick-bedded (0.5–1.5 m), cross-bedded and laminated calcarenites.

Intra-peloid packstone/grainstone with bioclasts (B5): Peloids are the most abundant grains (~40 %), other grains consist of intraclasts (25 %) and bioclasts (15 %), the latter including echinoderms, brachiopods and foraminifera (Fig. 7e). Micritization has affected many fragments, leaving only ghost outlines. Intraclasts consist mostly of well-rounded but poorly sorted mud fragments and in places of bioclasts; their sizes range from ~0.8 to 1.5 mm. The clasticity index of intraclasts is about 1 mm. In outcrop, these strata appear as moderately cross-bedded and cross-laminated, fine- to medium-grained (mostly <1 mm), grey to buff-colored, thick-bedded (2–3 m) calcarenites.

Peloid-ooid grainstone (B6): Ooids (~35 %) are the major nonskeletal carbonate grain type. Well-sorted and rounded peloids make up ~25 %. The proportion of bioclasts is low (~3 %) and consists mostly of large brachiopod fragments and echinoderms (Fig. 7f). The clasticity index of ooids is ~0.7 mm. In the field, beds of this facies appear as fine-grained, light grey, thick-bedded (about 2–3 m) cross-bedded calcarenites.

Peloid-bioclast-ooid grainstone (B7): Skeletal and nonskeletal grains in this facies consist of echinoderms, brachiopods, bivalves, and a low proportion of bryozoans (totally ~20 %), peloids (~15 %), ooids (~15–20 %), and some aggregate grains (<1 %) (Fig. 7g). Medium-sized calcite crystals fill interstices. Ooids display radial and tangential fabrics and are in places micritized in their centers. Some bivalves and brachiopods exceed 2 mm in diameter. In outcrop, this rock type forms thick-bedded (about 2 to >3 m), grey to tan, in places cross-bedded limestones.

Interpretation Oolitic and bioclastic shoals commonly separate restricted lagoonal environments from deeper ramp environments (Flügel 2010) and may act as wide and extensive barriers to currents and waves. In this context,

bioclastic and intraclastic pack- and grainstones and peloidal limestones with sparry calcite cements, cross-lamination and lacking significant mud in facies B4, B6, and B7 indicate an intermediate position between low- and high-energy conditions. The well-sorted, cross-laminated peloid grain-/packstones (B1) with a low proportion of agglutinating foraminifera (miliolids and textulariids) and bivalve and brachiopod fragments may represent moderate- to high-energy environments (Wilmsen et al. 2010); they even may indicate a temporary interruption of sediment accumulation (Hips and Haas 2009).

Intraclastic pack- to grainstones of facies B3 (largely bio- and intrasparites) may represent the highest-energy shallow environments. These deposits likely formed due to storm wave erosion and reworking of various shallow-marine sediments (Flügel 2010). This facies is comparable to SMF14 and RMF11 of Wilson (1975) and Flügel (2010), respectively. The abundance and high diversity of skeletal fauna (such as echinoderms, bryozoans, brachiopods, and bivalves) in facies B4 and B7 implies normal-marine conditions and distinguishes them from the facies in supratidal, intertidal, and restricted platform areas (e.g., Jank et al. 2006). The presence of poorly sorted and poorly rounded intraclasts (ranging in size from <1 to >2 mm) and peloids with sparry cement (B5) is characteristic of channels cutting through shoals (Tucker and Wright 1990). Bioclastic-ooid grainstone (B7) and the thin, occasionally graded beds of ooid grainstone (B2) with variable proportion of bioclasts (mainly bivalve, echinoderm and brachiopod fragments) and presence of cross-beds in these facies (B2 and B7) indicate deposition in relatively high-energy shoal environments with normal marine conditions, including shoreface and foreshore sub-environments (e.g., Azeredo et al. 2002; Cortes et al. 2009). The radial ooids (about 5–10 mm in diameter) indicate elevated energy settings (storms, high tides and waves; Wilmsen et al. 2010). This facies is comparable to the barrier-margin facies SMF15 and RMF29 of Wilson (1975) and Flügel (2010), respectively.

Ooids in facies B2 differ from those in the B4 and B6 facies. In B2, they resemble type 1 ooids whereas ooids of facies B4 and B6 resemble type 3 and 4 ooids, which Strasser (1986) described in Purbeck (lowermost Cretaceous) limestones of the Swiss and French Jura. Preferential dissolution of type 1 ooid cortices indicates an unstable primary composition. These ooid types occur together with marine fauna and thus likely indicate a high-energy sand-bar setting in normal-marine waters (Strasser 1986). Late Jurassic peloids have also been reported from Poland (Matyszkiewicz et al. 2004), Romania (Herrmann 1996), and offshore Morocco (Steiger and Cousin 1984).

Thick oolite packstone–grainstone successions are commonly deposited in high-energy, shallow subtidal

environments or on adjoining mid-ramps (e.g., Schlager 2005; Hips and Pelikan 2002; Fürsich et al. 2003; Adabi et al. 2010) where they may interfinger with wackestones and finer-grained fossiliferous mudstones of more distal environments (Decarlis and Lualdi 2009). Overall, based on faunal and lithological composition, facies group B is part of a high-energy inner ramp.

Open marine

The open-marine facies group O1 to O8 mainly consists of fossiliferous marls to rudstones with a high diversity of skeletal components.

Bioclast-intraclast packstone/grainstone (O1): Intraclasts (~25 %) and bioclasts (~20 %) compose the principal grains of this facies. Peloids, bivalves, echinoderms and bryozoan fragments are present (Fig. 8a). Some bioclasts are micritized. In the field, beds of this facies appear as thin-bedded, occasionally graded calcarenites.

Bioclast rudstone (O2): Bioclasts typically represent ~20–30 % but exceed in places 50 %. They include brachiopods, echinoderms, bivalves, bryozoans, and coral fragments. Nonskeletal grains are rare and consist of small intraclasts (~3 %) (Fig. 8b). More than 10 % of bioclasts exceed 2 mm in diameter; they are affected by compaction and fracturing. Beds of this facies form medium- to coarse-grained, light grey to white, medium- to thick-bedded (0.2–1 m) calcarenites in the field.

Peloid-bioclast-intraclast packstone/grainstone (O3): Principal grain types include intraclasts (30 %), bioclasts (20 %), and peloids (15 %) (Fig. 8c). Bioclasts are composed of bivalves, brachiopods, corals, and echinoderms, which in places exceed 2 mm in diameter. Strata of this facies appear in the field as medium- to coarse-grained, grey, medium-bedded calcarenites with calcite veins.

Bioclast-oid wackestone (O4): Ooids and bioclasts are major grain types in facies O4. Radial ooids (~30 %) include single and composite types; they are in part affected by micritization (Fig. 8d) or by microboring organisms. Bioclasts include bivalves (~15 %) and bryozoans (~1–2 %). These calcarenites are fine-grained, in places laminated and bioturbated, tan to light grey, and thick-bedded.

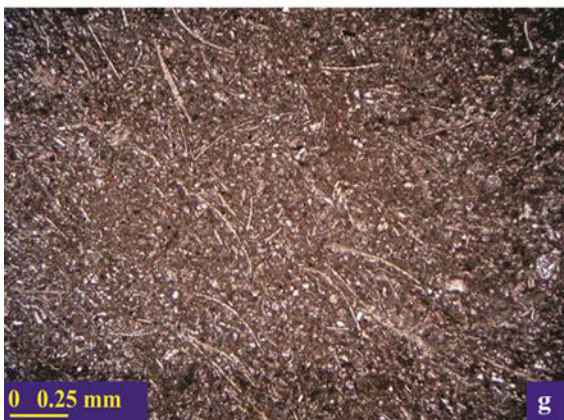
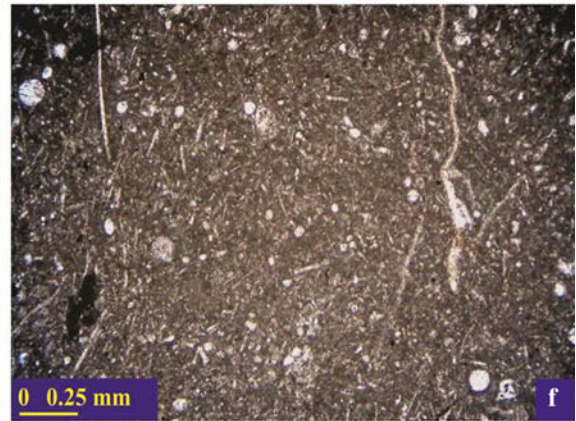
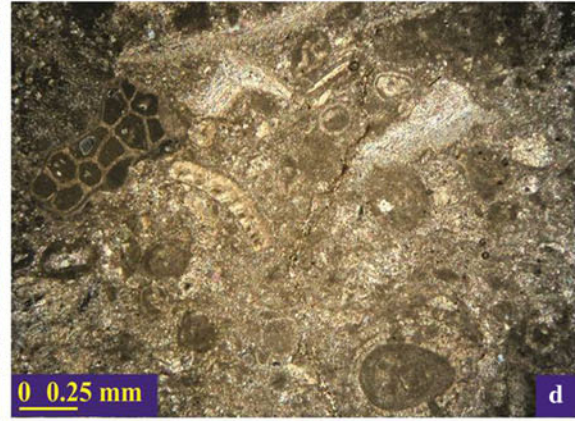
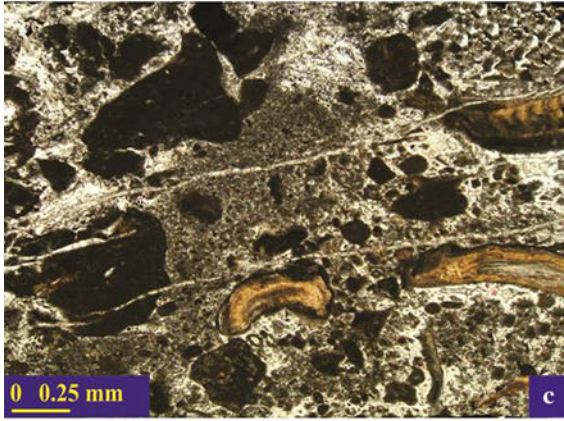
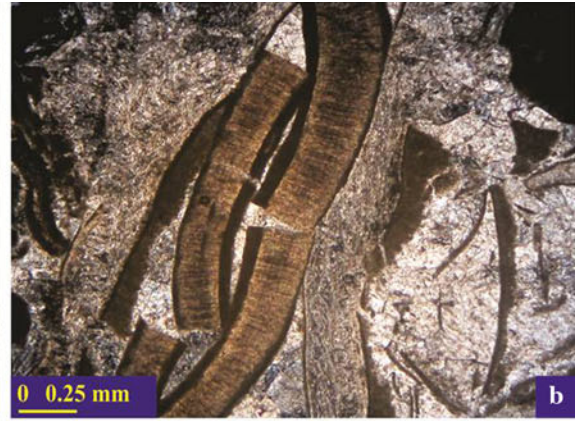
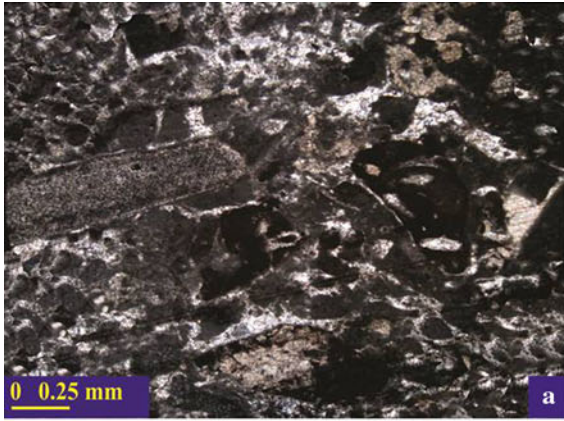
Deep-marine fossiliferous mudstone (O5): This facies is composed of fine-grained, relatively homogeneous, massive or poorly laminated, grey to buff-colored mudstone with scattered brachiopod and echinoderm fragments (Fig. 8e).

Radiolarian bivalve wackestone/packstone (O6): The abundance of radiolaria and thin bivalve fragments reaches ~20 and ~40 %, respectively. In the field, this is a fine-grained, laminated, buff-colored and medium-bedded (0.2–0.5 m) calcilutite with slightly nodular, thin chert nodules (Fig. 8f).

Pelagic bivalve wackestone (O7): Grain types of this facies are mainly composed of thin fragments of pelagic bivalve shells (~25–30 %) and 3–5 % radiolarians (Fig. 8g).

Ammonite-bearing marl (O8): These deposits are present particularly in the lower parts and near the base of the measured sections. They are grey to light grey, occasionally laminated, ammonite-bearing marls with occasional sponge spicules and pelagic bivalves. Beds of this facies are interbedded with open- to deep-marine wackestone (O6, O7) and fossiliferous mudstones (O5) (Fig. 8h).

Interpretation The presence of open-marine fossils (brachiopods, echinoderms, ammonites, pelagic bivalves and radiolarians), of mud-supported facies, and the corresponding lack of high-energy facies all show that these deposits formed in relatively low-energy open-marine environments (Fig. 9; Pomar 2001a, b; Alsharhan and Kendall 2003; Cosovic et al. 2004). In the deeper part of the ramp, carbonate facies changes from grainstone (O1, O2 and O3) and wackestone/packstone (O4–O7) to mudstone (O5), and in places to deep-marine marl (O8). The bioclastic limestones (O1–O3) formed in warm, well-oxygenated, inner and proximal mid-ramp environments of normal salinity (Hips and Haas 2009) which offered appropriate conditions for crinoids (Martini et al. 2007), while carbonate mud was transported offshore by storm currents. The mud-supported fabric of facies O4–O7, in contrast, suggests mid- and outer-ramp deposition in greater water depth. The presence of coated bioclasts with micrite envelopes in facies O1, O3, and O4 indicates that skeletal and nonskeletal grains derived from shallow environments were transported in deeper water by offshore-directed bottom currents during waning storms (Martini et al. 2007). Strong micritization of bioclasts, especially of echinoderms, without observed change of environments may imply a break in carbonate sedimentation. The fine-grained bioclastic mudstone (O5) and wackestone (O6) is interpreted as having accumulated under episodic turbulence or the occasional influence of strong currents below fair-weather wave-base (Buckovic et al. 2001; Jank et al. 2006). However, the near-absence of storm- or wave-generated structures in most facies of group O, the largely massive texture of the mudstone in the mud-dominated facies (O4–O7) without well-defined sedimentary structures, and the rarity of individual peloids, micritized bioclasts, and ooids also suggest widespread low-energy environments below storm wave base (sensu Burchette and Wright 1992; Hips and Haas 2009; Wilmsen et al. 2010). The abundance of stenohaline fauna such as bryozoans, echinoids, and brachiopods (O1–O5) and stratigraphic relationships with adjacent facies in these facies conforms to this interpretation (Pomar 2001a, b;



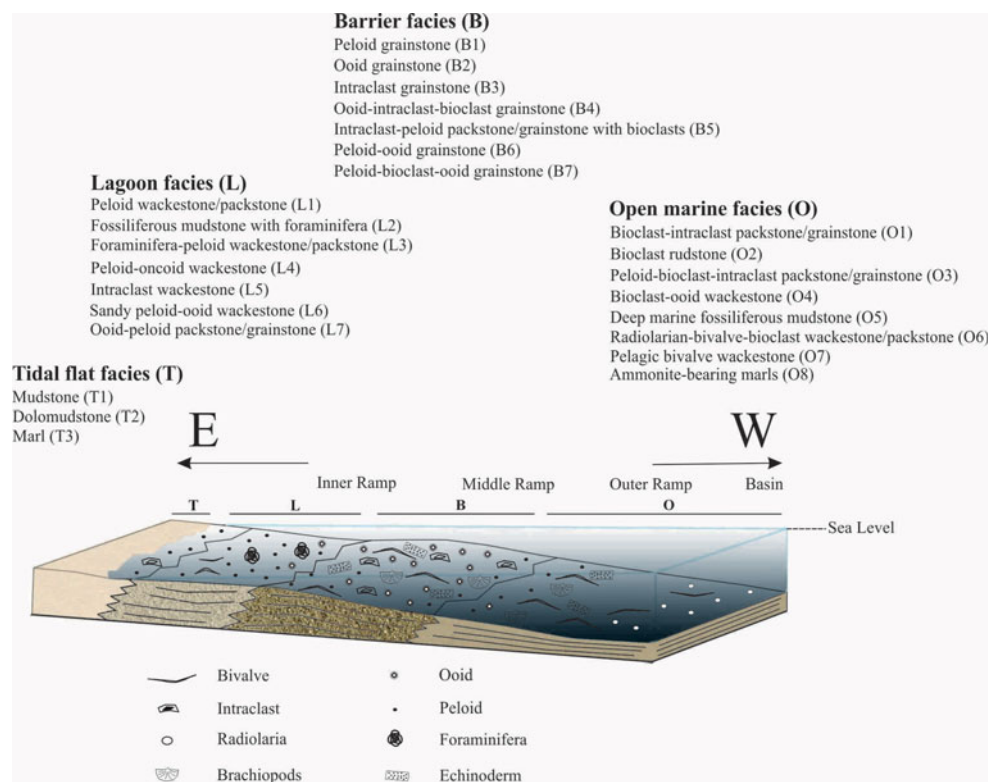
◀ **Fig. 8** Thin-sections (a–g) and field photograph (h) of open-marine facies. **a** Bioclast-intraclast packstone/grainstone with echinoderm and bivalve fragments, Garmeh section (O1). **b** Brachiopod-echinoderm bioclast rudstone, Ziarat section (O2). **c** Peloid-bioclast-intraclast grainstone with subangular intraclast, bivalve and brachiopod fragments, Kotali section (O3). **d** Bioclast-oid wackestone, Kotali section (O4). **e** Deep-marine fossiliferous mudstone, Jorbat section (O5). **f** Radiolarian-bivalve bioclast wackestone/packstone, Ziarat section (O6). **g** Pelagic bivalve bioclast wackestone, Ziarat section (O7). **h** Ammonite-bearing marls, Jorbat section (O8). *Hammer* for scale

Cosovic et al. 2004). Based on the presence of stenohaline bioclasts such as brachiopods, echinoderms, and bivalves, mudstones of facies O6 were deposited in low-energy open-marine environments (Alsharhan and Kendall 2003). Partial silicification of carbonate grains in facies O6 and O7 produced nodules and lenses of grey to buff-colored microquartz, likely due to diagenetic dissolution of siliceous sponges and radiolaria (Claps et al. 1996; Cozzi 2002). Finally, the marly facies (O8) can be attributed to open-marine conditions, based on its skeletal grain types (ammonites, sponge spicules, and pelagic bivalves) and its interbedding with deep-marine fossiliferous mudstones and bioclastic wackestones (O5 and O6, Fig. 9).

Sequence stratigraphy

Sequences can be the result of eustatic sea-level fluctuations and/or tectonic movements at different temporal and spatial scales and can be produced by a variety of processes

Fig. 9 Depositional model of Upper Jurassic carbonates in the study area

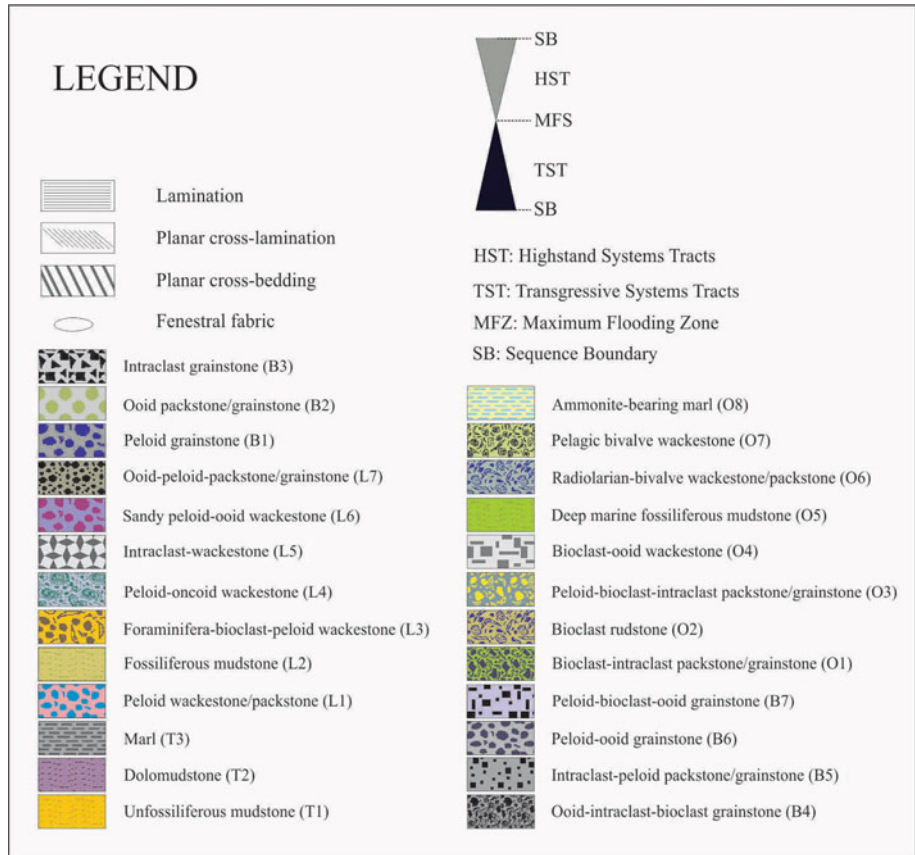


(Brunet et al. 2009) which will affect the architecture of the stratigraphic record (e.g., Fürsich et al. 2003; Catuneanu et al. 2009). The common shallowing-upward cycles in some units in the study area indicate sedimentary responses to relative sea level change ranging from deep water to tidal flat environments.

Based on their relative position with respect to other environments, we interpreted facies and facies groups within the studied sequences as follows: Sequence-stratigraphic surfaces (SB) are mainly located in tidal flat and lagoonal facies. Fluvial deposits and major erosional surfaces characteristic of lowstand system tracts (LST) were not observed within the studied successions but may be represented by sandstones, siltstones, mudstones and marls interbedded with evaporites further to the east (e.g., Kavooosi 1990). Transgressive surfaces (TS) are mostly located within peloid packstone/grainstone (B1), intraclastic pack- to grainstone (B2), and, in places, by peloid-bioclast-intraclast packstone/grainstone (O3).

The erosional contact between underlying marls to overlying conglomerates (or to red sandstones in the Garmeh section) at the top of all stratigraphic sections clearly represents a first-order discontinuity which has been interpreted as an erosional sequence boundary (SB1) (e.g., Jank et al. 2006; Zagrarni et al. 2008). Below the capping contact, we identified four depositional sequences marked by nonerosional boundaries (except DS4) (Figs. 10, 11, 12, 13, 14).

Fig. 10 Facies symbols and abbreviations for Figs. 11, 12, 13, 14, 15



Depositional sequence 1 (DS1)

Depositional sequence (DS1) starts with a transgressive phase (TST). In the Ziarat section (Fig. 11), this TST consists of barrier and shallow, open-marine peloid-bioclast-intraclast packstone, bioclast wackestone, fossiliferous mudstone with echinoderm and brachiopod fragments at the base, and grades into deep-marine mudstones representing the maximum flooding zone (MFZ) (Fig. 11). At the Kotali section (Fig. 12), the same interval consists of shallow, open-marine peloid packstone with bivalve fragments and a low proportion of echinoderm fragments at the base, overlain by relatively deep-marine bioclast wackestone and deep-marine fossiliferous mudstone containing open-marine bioclasts such as bivalves, brachiopods, and echinoderms. This last unit presents a MFZ (Fig. 12). In the West Kotali section (Fig. 13), DS1 begins with open-marine and barrier peloid-bioclast and intraclast packstone/grainstone and fossiliferous mudstones, alternating with deep-marine fossiliferous mudstones; the latter representing the MFZ (Fig. 13). At the Jorbat and Garmeh sections (Figs. 14, 15), DS1 includes barrier and open-marine bioclast peloid and intraclast packstone, overlain by thin, deep-marine bivalve-fragment, radiolaria and sponge spicule wackestones, and finally by deep-marine marls

(O8) and fossiliferous mudstones (O5); the last rock type represents the maximum flooding zone (MFZ) (Figs. 14, 15).

The highstand systems tract (HST) of DS1 is characterized in the Ziarat area by open-marine bioclast-peloid packstone/grainstone with echinoderm, coral, and bivalve fragments, and barrier-facies intraclast peloid packstone/grainstones that are overlain by unfossiliferous tidal flat mudstones (Fig. 11). In the Kotali area, the same HST is characterized by a progradational package of lagoonal and barrier intraclast-peloid packstone with brachiopod, echinoderm, and bivalve fragments, peloid packstone, ooid grainstone, ooid-peloid packstones and finally tidal-flat unfossiliferous mudstones (Fig. 12). In the west Kotali section, lagoonal and barrier peloid-bioclast and intraclast packstone/grainstone and fossiliferous mudstone were deposited on top of open-marine fossiliferous mudstones; the former grade upwards into unfossiliferous mudstones (Fig. 13). In the Jorbat section, the HST of DS1 is composed of deep-marine mudstones, which are overlain by shallow-marine bioclast wackestones and finally lagoonal peloid and bioclast wackestones with bivalve and foraminifer fragments (Fig. 14). At the Garmeh section, fossiliferous mudstones and bioclast wackestones with open-marine bioclasts (bivalves, brachiopods and echinoderms) are

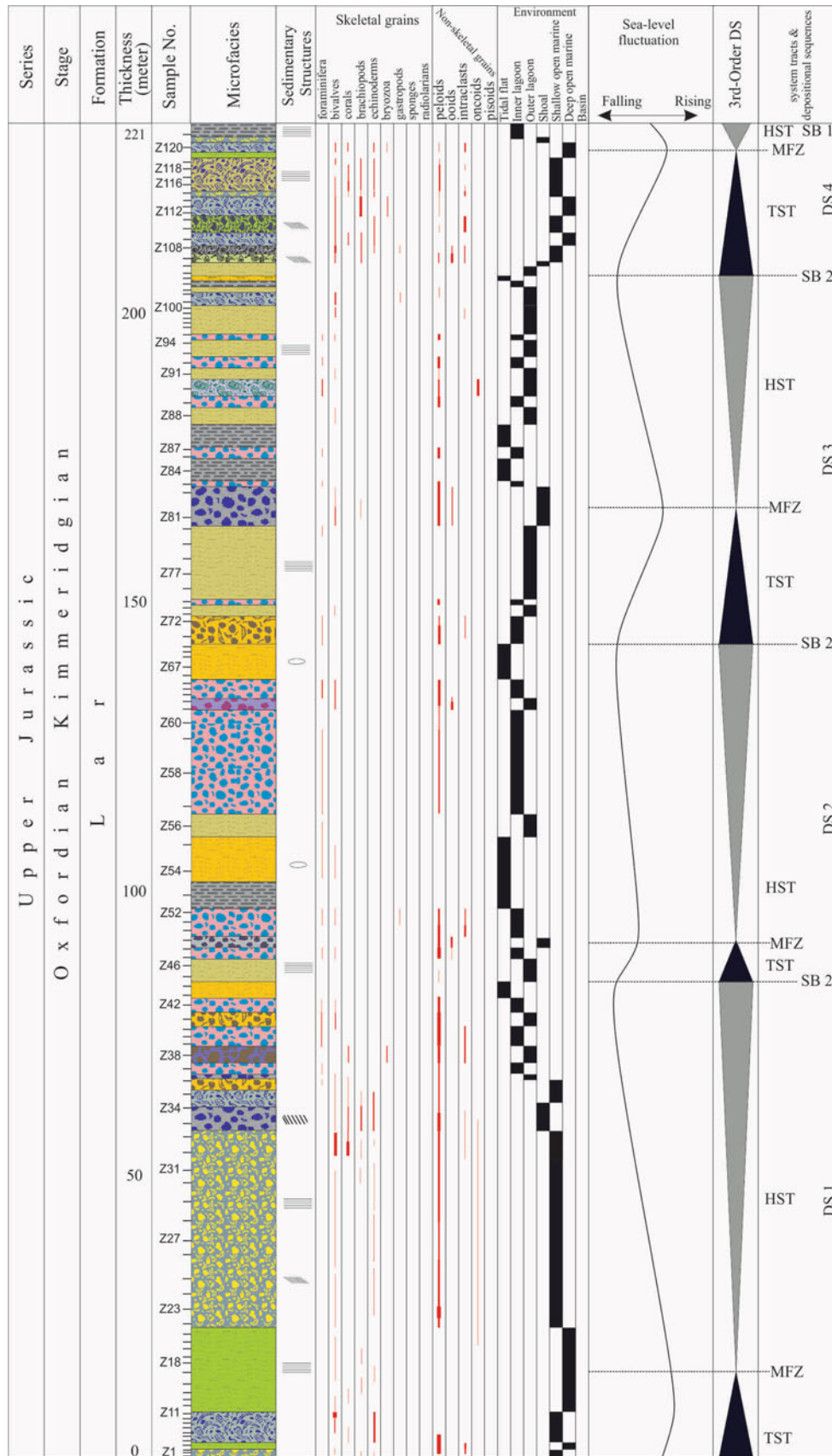


Fig. 11 Lithology of Upper Jurassic carbonates of the Ziarat section and its sequence-stratigraphic interpretation

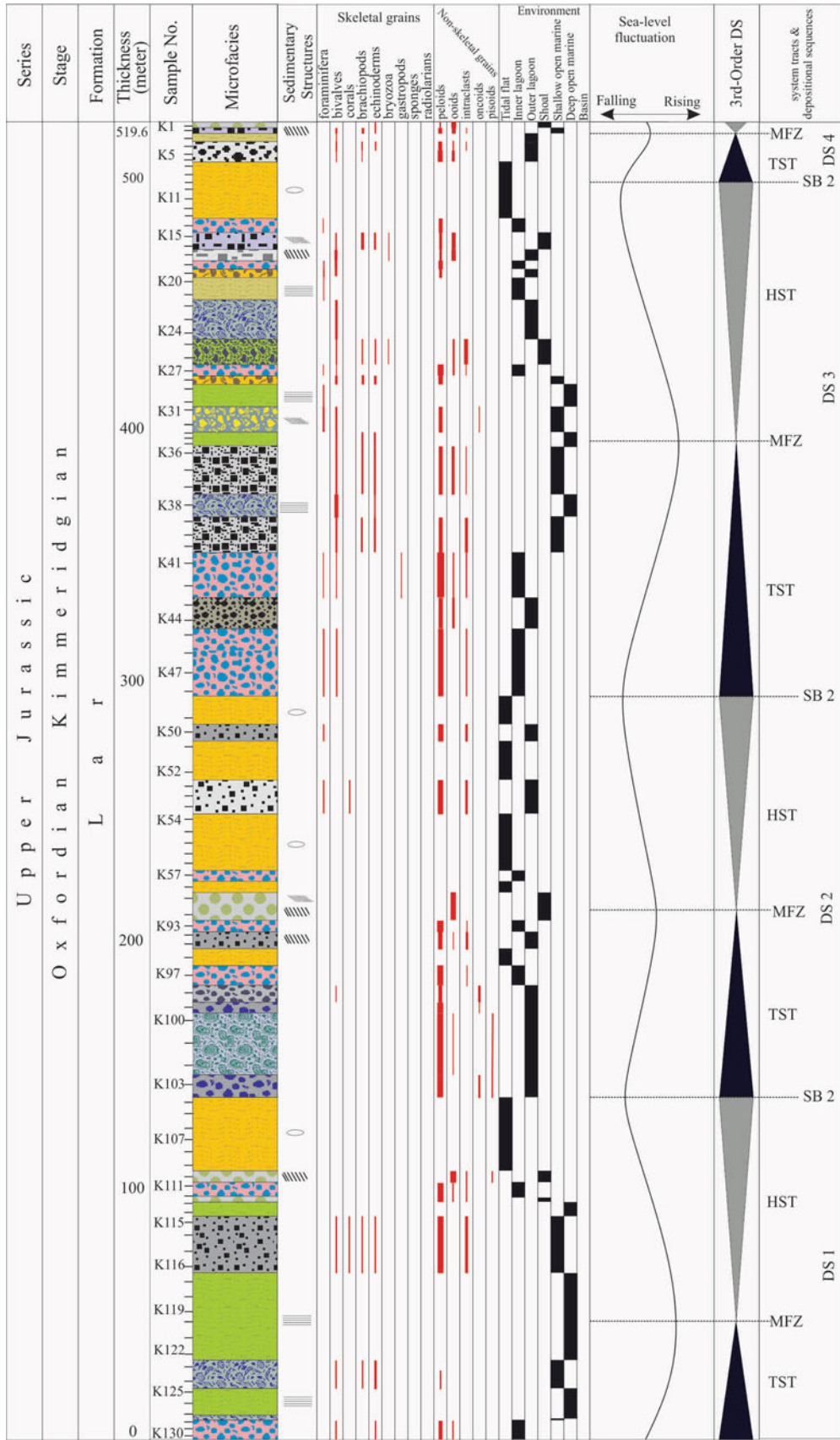


Fig. 12 Lithology of Upper Jurassic carbonates of the Kotali section and its sequence-stratigraphic interpretation

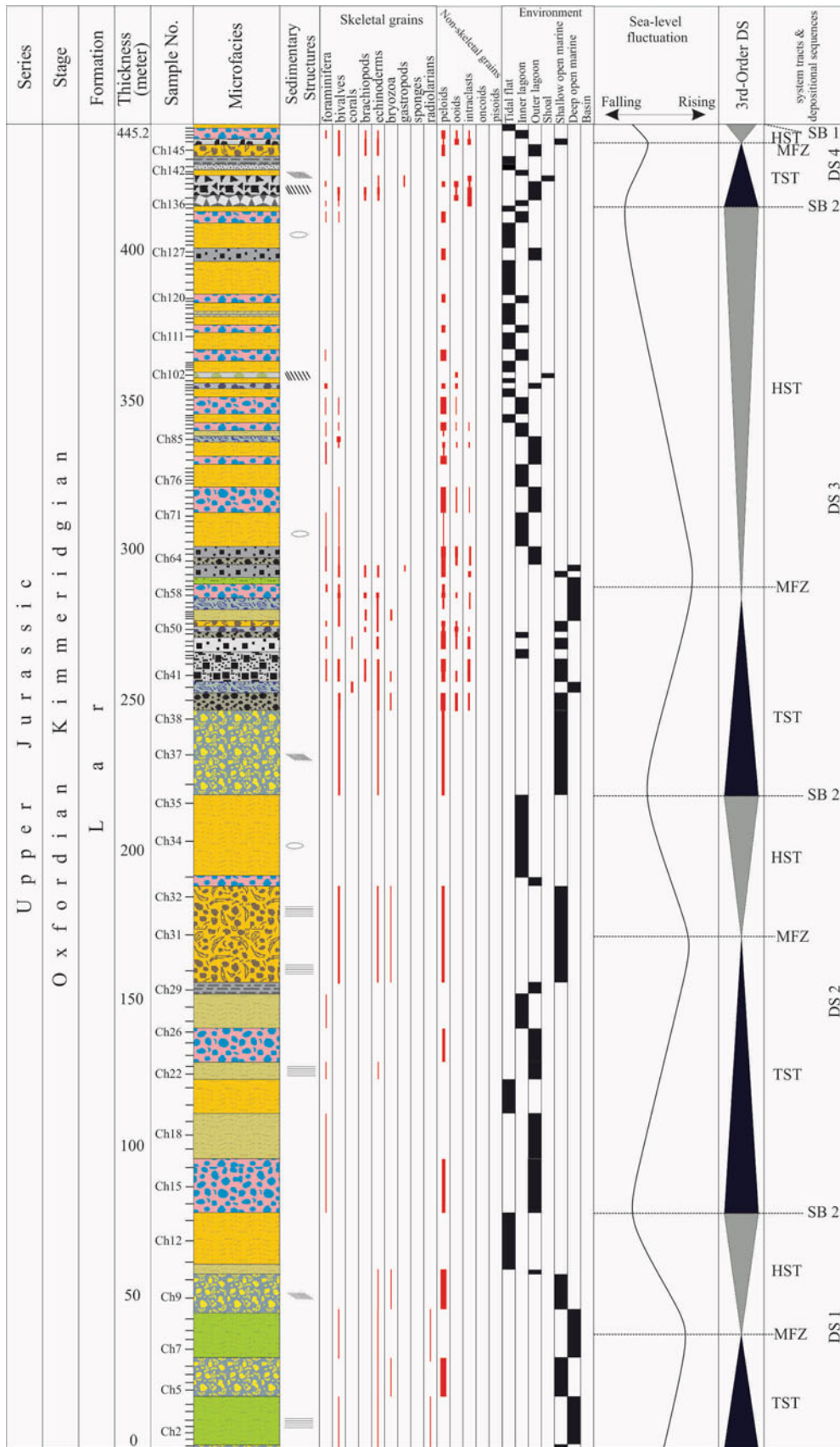


Fig. 13 Lithology of Upper Jurassic carbonates of the West Kotali section with its sequence-stratigraphic interpretation

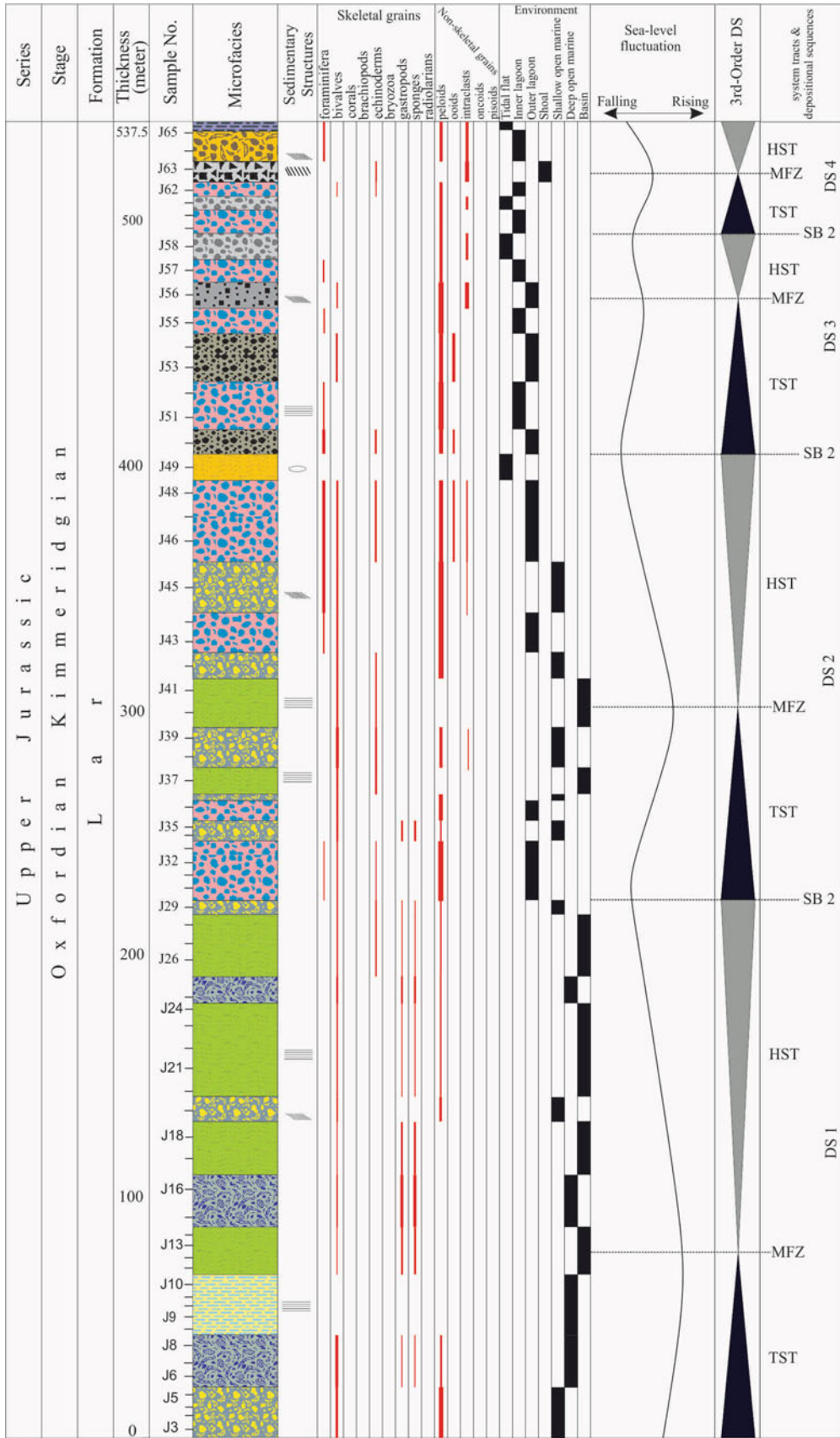


Fig. 14 Lithology of Upper Jurassic carbonates of the Jorbat section with its sequence-stratigraphic interpretation

overlain by shallow-marine and lagoonal facies. The contact between DS1 and DS2 is of the SB2 type (Fig. 15).

Depositional sequence 2 (DS2)

The transgressive systems tract (TST) of DS2 in the Ziarat section is marked by deposition of barrier peloid-oid grainstone and lagoonal facies such as peloid packstones (with bivalve fragments) on top of tidal-flat unfossiliferous mudstones (Fig. 11). In the Kotali section, equivalent deposits consist of barrier peloid grainstone, peloid-oid grainstone, intraclast peloid packstone, and peloid wackestone/packstone. Topmost ooid grainstone represent the MFZ (Fig. 12). In the West Kotali section, the lagoonal facies consists of peloid wackestones/packstone and fossiliferous mudstone with miliolids, textulariids, and tidal-flat unfossiliferous mudstone which are overlain by lagoonal bioclast-peloid wackestone/packstone with bivalve, bryozoan, and echinoderm fragments. This last rock type marks the MFZ (Fig. 13). In the Jorbat section, the MFZ consists of deep-marine fossiliferous mudstones with bivalves, echinoderm spines and radiolarians; the same zone is represented in the Garmeh section by barrier and open-marine peloid-bioclast and intraclast packstone/grainstone that were deposited on top of lagoonal peloid packstone, mudstone, and bioclast-peloid wackestone pertaining to the TST (Figs. 14, 15).

The HST of DS2 in the Ziarat and Kotali sections is characterized by a progradation from lagoonal and barrier facies to an unfossiliferous tidal-flat facies (Figs. 11, 12). In the West Kotali section, this HST consists of lagoonal and tidal-flat peloid wackestones/packstones and unfossiliferous mudstones that were deposited on top of deeper-water facies (Fig. 13). In the Jorbat section, the HST is represented by lagoonal and barrier peloid-bioclast-intraclast packstone, peloid packstone, bioclast-peloid grainstone with foraminifera and rare bivalves at the base, which were overlain by tidal-flat unfossiliferous mudstones (Fig. 14). In the Garmeh section, the deposits resemble those at Jorbat: An open-marine peloid wackestone/packstone facies containing bivalves, gastropods, and miliolids alternating with bioclast wackestones is overlain by tidal-flat unfossiliferous mudstones (Fig. 15).

Depositional sequence 3 (DS3)

At the Ziarat section, the TST of DS3 starts with lagoonal peloid wackestone/packstone (L1), fossiliferous mudstone (L2) and peloid-oid wackestone (L4) alternating with tidal-flat marls (T3) which underlie barrier-facies peloid grainstone (B1). The MFZ is marked by peloid grainstone with bivalves, brachiopods, and rare gastropods (Fig. 11). At the Kotali section, DS3 is represented by lagoonal

peloid and ooid packstone, bivalve and foraminiferal packstone, and by lagoonal and barrier bioclast and peloid-intraclast packstone/grainstones. These are overlain by open-marine bioclast wackestone and fossiliferous mudstones bearing bivalve, echinoderm, and brachiopod fragments, marking the MFZ (Fig. 12). In the West Kotali section, the TST is recognized by lagoonal peloid and bioclast wackestones and by barrier- and open-marine peloid-bioclast-oid grainstone and peloid-bioclast-intraclast packstone/grainstones with bivalve and echinoderm fragments. The TST is overlain by deep-marine mudstone with echinoderms and brachiopods (MFZ) (Fig. 13). In the Jorbat section, lagoonal strata occur below a subtidal barrier facies with echinoderm and brachiopod fragments, representing the MFZ (Fig. 14). At the Garmeh section, deep-marine fossiliferous mudstones marking the MFZ were deposited on top of shallow-marine bioclast wackestones and bioclast-peloid packstones of the TST (Fig. 15).

The HST of DS3 in the Ziarat section includes common shoaling-upward parasequences which consist of peloid packstone (L1), marl (T3), and peloid-oid wackestone/packstone (L4) that are progradationally overlain by tidal-flat marl and mudstone (T1 and T3) (Fig. 11). In the Kotali section, the HST facies starts with open-marine peloid-bioclast-intraclast packstone/grainstone and bioclast-intraclast grainstone that continue upward with lagoonal and barrier bioclast-peloid packstone, intraclast and bioclast packstone/grainstone containing bivalve and foraminifera, fossiliferous mudstone and wackestone, and peloid wackestone. These are covered by tidal-flat peloid packstones and mudstones (Fig. 12). In the West Kotali section, the HST is marked by regressive facies and shallowing-upward parasequences, composed mainly of lagoonal peloid-intraclast wackestone, peloid-bioclast wackestone with benthic foraminifera (miliolids) and intraclast wackestone that were deposited on top of open-marine facies (Fig. 13). In the Jorbat section, the HST consists of regressive parasequences from barrier peloid-intraclast packstone/grainstone and peloid-oid grainstone to shallow-water lagoonal peloid packstone (Fig. 14). In the Garmeh section, the HST deposits consist of lagoonal and barrier bioclast-peloid packstone and intraclast packstone with peloid and open-marine bioclasts (bivalves, echinoderms and brachiopods) that are overlain by shallow-marine lagoonal and tidal flat peloid wackestone and mudstones (Fig. 15).

Depositional sequence 4 (DS4)

The TST of DS4 shows a retrogradation from lagoonal fossiliferous mudstone and high-energy barrier-facies ooid-intraclast grainstone with some open-marine bioclasts to deep-marine bioclast wackestone and mudstone, the latter

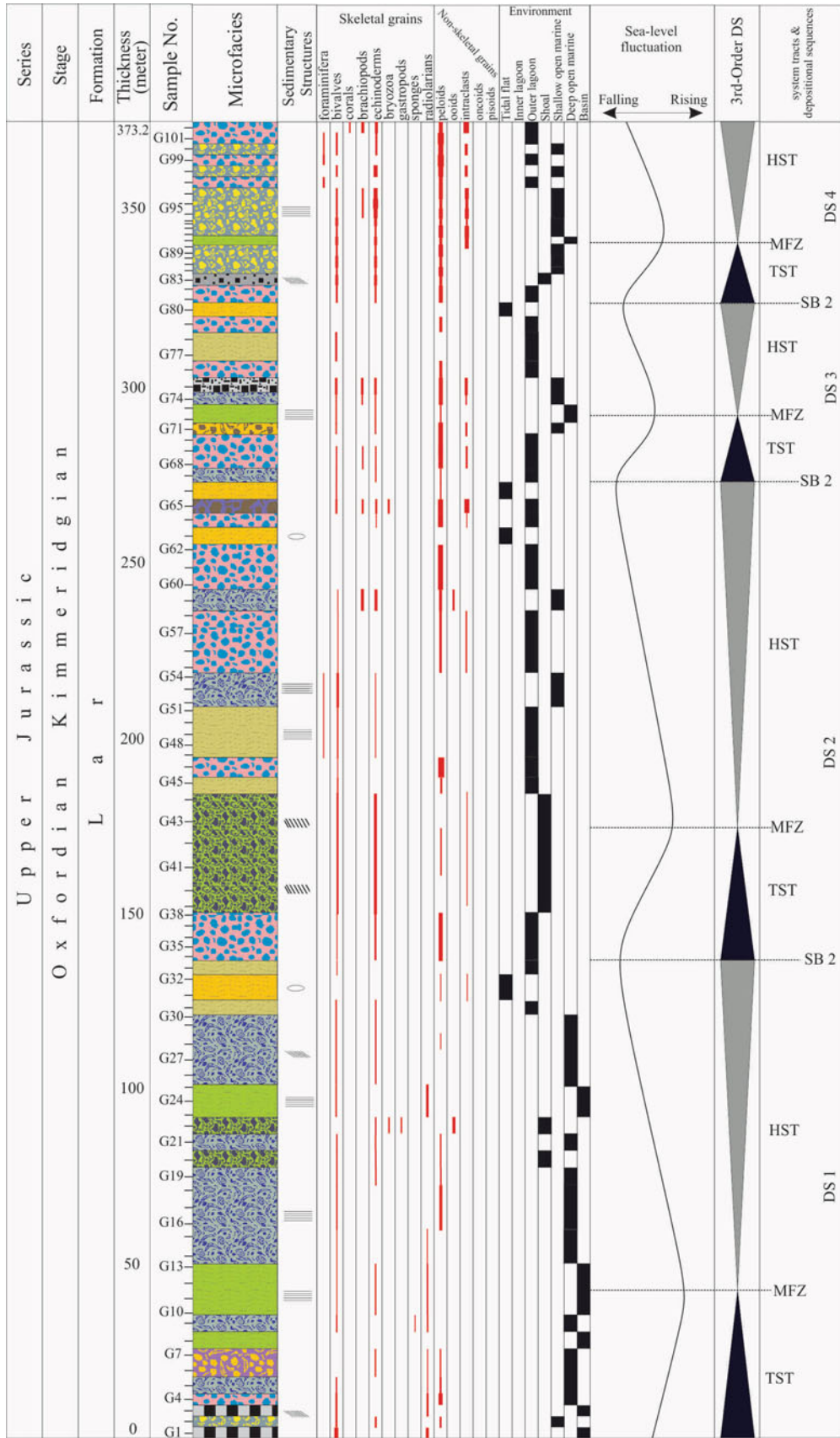


Fig. 15 Lithology of Upper Jurassic carbonates of the Garmeh section and its sequence-stratigraphic interpretation

representing the MFZ (Fig. 11). In the Kotali section, there is a transgression from tidal-flat mudstone and lagoonal and barrier peloid-oid grainstone, bioclast-peloid packstone/grainstone containing bivalve and brachiopod fragments to open-marine mudstones marking the MFZ. In the West Kotali section, the TST consists of shallow-marine lagoonal and barrier-facies intraclast wackestone/packstone, bioclast grainstone, ooid and intraclast grainstone and ooid packstones at the base to open-marine bioclast packstone/grainstones with echinoderm and brachiopod fragments, the latter denoting the MFZ (Fig. 13). In the Jorbat section, the TST is distinguished by lagoonal peloid wackestones/packstone overlain by barrier peloid and ooid packstone. These are, in turn, overlain by high-energy, open-marine intraclast grainstone marking the MFZ (Fig. 14). At Garmeh, shallow-water, semi-restricted peloid packstones and bioclast packstones are underlain by barrier bioclast and intraclast packstone/grainstones and shallow open-marine bioclast wackestone containing echinoderm and brachiopod fragments, respectively. These two facies represent the TST and are overlain by deep-marine mudstone (MFZ) (Fig. 15).

During the HST of DS4, the degree of restriction increased in the platform interior so that mud-rich facies accumulated in expansive lagoons and on tidal flats. Deposits in the Ziarat section include shallow-water marls on top of deeper-water open-marine bioclast wackestones. In the Kotali section, the HST is characterized by regression from deep-marine mudstones to shallow-marine, higher-energy barrier ooid and peloid-oid grainstones (Fig. 12). In the West Kotali section, the HST consists of tidal-flat dolomitized unfossiliferous mudstone and lagoonal peloid wackestone with bivalves and foraminifera and peloid-intraclast packstone with gastropods and bivalves. They overlie bioclast and ooid grainstones containing open-marine-facies bioclasts (Fig. 13). In the Jorbat section, the HST of DS4 is distinguished by progradation of facies belts from lagoonal peloid and bioclast wackestone with bivalves and foraminifera to tidal-flat marls (Fig. 14). In the Garmeh section, lagoonal and restricted strata overlie deep-marine facies (Fig. 15). These HST deposits are unconformably overlain by Lower Cretaceous red sandstones and conglomerates (Fig. 11).

Interpretation of sequences and relative sea level changes

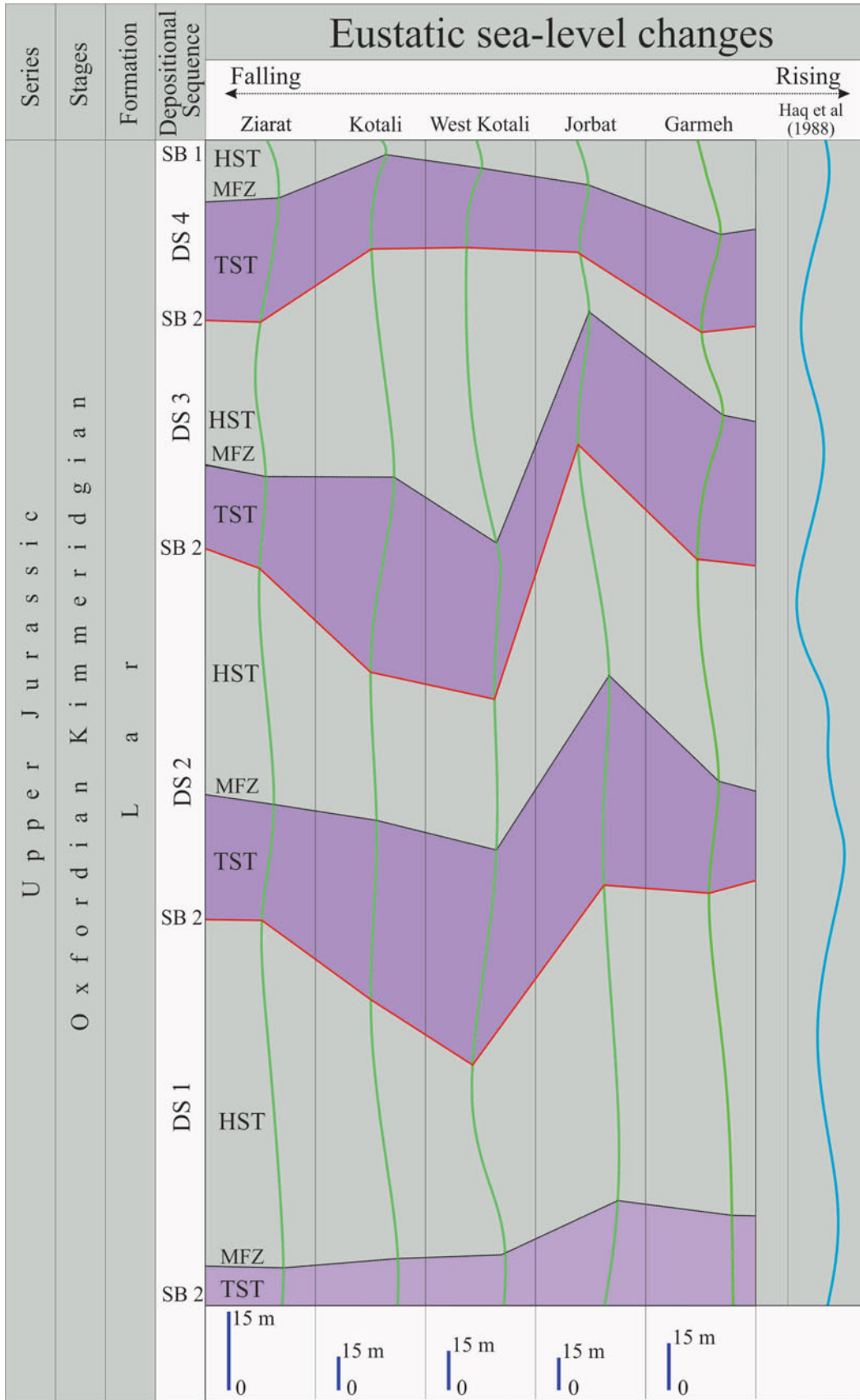
The TST of DS1 at the base of all sections shows deposition of relatively deep-water marl, lime mudstones and open-marine carbonates on shallow-water carbonates. These are mostly barrier- and deep-marine facies that were deposited on lagoonal and tidal-flat facies and show a deepening-upward trend. The boundaries between Middle

and Upper Jurassic strata at the base of the sections and of the overlying four depositional sequences are gradational and nonerosional (SB2) (Fig. 16), while the boundary between Upper Jurassic and Lower Cretaceous deposits at the top of all sections is of SB1 type. Some of the TST show gradual deepening-upward parasequences from shallow-marine deposits (skeletal and nonskeletal packstone/grainstone) to deep-marine wackestone and fossiliferous mudstone. Late TST and early HST facies are usually deposited in low-energy environments below fair-weather wave base but locally represented also relatively high-energy barrier and semi-restricted lagoonal environments. HST deposits generally show shallowing-upward trends from relatively deep-marine (skeletal packstones and wackestones), barrier (skeletal and nonskeletal grainstones) to lagoonal and tidal-flat deposits (e.g., Spengler and Read 2010).

Sequence-stratigraphic correlation of the sections show that the TST in the first depositional sequence (DS1) starts with barrier and open-marine facies that are overlain by deep-marine mudstones and marls. The HST of DS1 at Ziarat, Kotali and West Kotali consists of a shallowing-upward trend from lagoonal and barrier facies that are overlain by tidal-flat deposits. At Jorbat and Garmeh, the regression is less pronounced; there, tidal-flat deposits are not observed. Lagoonal and barrier-facies predominate. The TST of DS3 is marked by deposition of lagoonal and barrier on tidal-flat facies, overlain by open-marine facies. Progradation occurred during the HST so that tidal, lagoonal and barrier-facies overlie open-marine facies. Near the top of the sections, the TST of DS4 shows lagoonal and barrier facies overlain by open-marine facies, prior to the marked marine regression which terminated carbonate deposition.

Sequence-stratigraphic correlation and the occurrence of key facies suggest a deepening trend from Ziarat and Kotali in the east to Jorbat and Garmeh in the west. Overall, the high proportion of tidal-flat, lagoonal and barrier facies demonstrates relatively shallow-water conditions. The westward-deepening trend is consistent with the observation of Late Jurassic LST in the Kopet Dagh Basin to the east of the study area which include correlative sandstones, siltstone, red marls and evaporites (Kavoosi et al. 2009).

The interpretation of observed relative sea level changes in stratigraphic sequences always demands the consideration of tectonic versus eustatic control. The type-1 sequence boundary at the top of all measured sections, which places terrestrial siliciclastics on platform carbonates, can be regionally observed and is clearly related to folding and deformation (Neocimmerian orogenic event; Fürsich et al. 2003; Wilmsen et al. 2003, 2009b, 2010; Seyed-Emami et al. 2004) which reflects accretion of various tectonic blocks now in Iran, Afghanistan and



◀ **Fig. 16** Correlation chart showing changes in thickness between depositional sequences in the measured stratigraphic sections in the eastern Alborz and Binalud Mountains. Note change in scale for Ziarat section. Global sea-level changes of Haq et al. (1988) are shown on the right

Pakistan to Laurasia (e.g., Thomas et al. 1999). The Late Cimmerian tectonic events led to deposition of Lower Cretaceous continental siliciclastics (sandstones, conglomerates and evaporites) of the Shurijeh Formation in northeast Iran (e.g., Kavooosi et al. 2009). Deformation and uplift on the uplifted southern margin of the Scythian–Turan Platform during the Kimmeridgian and Tithonian is also well recorded by regression and associated facies changes (Kazmin 1989; Clarke 1994; Golonka 2004). All these facies shifts clearly represent the Late Cimmerian tectonic event which, however, coincides with a Latest Jurassic–Early Cretaceous global sea-level fall (Haq et al. 1981).

Whether the four Late Jurassic third-order cycles DS1 through DS 4 documented here are due to eustatic or tectonic control is therefore difficult to answer. Even though tectonic events may influence stratigraphic cyclicity at virtually any time scale (Catuneanu and Elango 2001; Davies and Gibling 2003; Catuneanu 2006), high-frequency relative sea-level changes are also caused by differences in carbonate production rates or by variable wave- and current-controlled sediment accumulation rates at changing water depths (e.g., James et al. 2001; Pedley and Carannante 2006; Nalin et al. 2008). Because we do not observe widely changing thicknesses of sedimentary units or abrupt facies changes in the study area which would point to local or regional tectonic instability, we rather suspect a regional change in the Late Jurassic rate of sea-level rise to have been the primary control on facies, depositional environments and stratigraphic architecture (Kavooosi et al. 2009; Van Buchem et al. 2010). Such inference is also supported by the plausible match of our detailed correlations with the global sea level curves of Haq et al. (1988, Fig. 16). Even though we cannot provide high-resolution biostratigraphic control on the sections, both Haq et al. (1988) and our sections both show four sea-level maxima during the Oxfordian and Kimmeridgian.

Oxfordian–Kimmeridgian sequence tracts followed by subsequent marked global sea level fall in the latest Jurassic and earliest Cretaceous, similar to those in the Alborz and Binalud Mountains described here, have been documented worldwide: In the western and southern Persian Gulf (Hanifa and equivalent formations; e.g., Al-Husseini 1997) and the Arabian platform, relative sea level continued to rise from Middle to Late Jurassic while carbonate sedimentation took place (Alsharhan and Magara 1995). Numerous basins in Europe, such as northern and northeastern Iberia (Aurell et al. 2003), southeastern

France (e.g., Jacquin et al. 1998), southern England, Greenland (e.g., Wignall 1994; Taylor et al. 2001; Hallam 2001) and southern Germany (e.g. Ruf et al. 2005; Biskaborn 2009) show similar trends. In addition, strata in New Zealand, the Himalayas, the Pakistan Salt Range, the central Andes of Argentina and northern Chile also show Late Jurassic regression marked by deposition of shallow-marine facies (Haq et al. 1988). In northern Afghanistan and parts of southern Turkmenistan, Uzbekistan, and Tajikistan, Middle to Upper Jurassic transgressive–regressive successions consist of mixed continental and marine Bathonian to Lower Kimmeridgian siliciclastics and carbonates overlain by regressive Upper Kimmeridgian–Tithonian evaporite-bearing clastics (Brookfield and Hashmat 2001). We thus conclude that eustatic rather than tectonic control played a dominant role in controlling carbonate depositional environments in the study area. The effects of local tectonics are comparatively minor, likely causing differential subsidence and the observed discrepancies in sea-level fluctuation (e.g., Aurell et al. 2003).

Conclusions

Upper Jurassic carbonates in northern and northeastern Iran are composed of fine- to medium-grained, thin- to thick-bedded carbonate facies including mudstone, wackestone, packstone, grainstones, and some rudstones. These formed in low- to high-energy carbonate ramp environments in tidal-flat, lagoonal, barrier and open-marine settings along the subsiding northern margin of the Iranian blocks, adjacent to a continental back-arc basin. Facies analysis based on dominant carbonate grain-size and the type and proportion of skeletal (bivalves, brachiopods, echinoderms, foraminifera, corals, and bryozoans) and nonskeletal grains (intraclasts, ooids, and peloids) in five measured sections allowed to differentiate twenty-five facies ranging from tidal-flat to open-marine environments. Their lateral and vertical distribution pattern suggests a homoclinal, westward-deepening ramp preserving four third-order depositional sequences (DS1–DS4) between a basal Middle-to-Late Jurassic boundary and a marked first-order erosional sequence boundary of Lower Cretaceous age. TST within each DS typically show lagoonal and barrier facies overlain by shallow- and deep-marine facies; the latter usually include the MFZ. During HST stages, deep- and shallow-marine facies were gradationally overlain by shallow-marine barrier and lagoonal facies in shallowing-upward trends, occasionally reaching into tidal-flat facies. Global eustatic changes likely acted as primary drivers of the observed relative sea-level changes.

Acknowledgments We would like to thank the logistical and financial support given to this study by the Department of Geology of

Ferdowsi University of Mashhad-Iran. Thorough and constructive reviews by Markus Wilmsen, Beatrix Badenas Lago, and Franz Fürsich greatly improved the manuscript.

References

- Adabi MH, Salehi MA, Ghabeishavi A (2010) Depositional environment, sequence stratigraphy and geochemistry of Lower Cretaceous carbonates (Fahliyan Formation), south-west Iran. *J Asian Earth Sci* 39:148–160
- Adachi N, Ezaki Y, Liu J (2004) The fabrics and origins of peloids immediately after the end- Permian extinction, Guizhou Province, South China. *Sediment Geol* 164:161–178
- Aghaei A, Mahboubi A, Moussavi-Harami R, Zabihi F, Nadjafi M (2012) Microfossil studies and age determination of Upper Jurassic deposits in Garmeh section, southwest Jajarm. 6th Symposium of Iranian Paleontological Society, Jolfa (in press) (in Persian)
- Aigner T (1985) Storm depositional systems. Dynamic stratigraphy in modern and ancient shallow-marine sequences. *Lect Notes Earth Sci* 3:1–174
- Alavi M (1991) Sedimentary and structural characteristics of the Paleo-Tethys remnants in northeastern Iran. *Geol Soc Am Bull* 103:983–992
- Alavi M (1992) Thrust tectonics of the Binalood region, NE Iran. *Tectonics* 11:360–370
- Alavi M, Vazir H, Seyed-Emami K, Lasemi Y (1997) The Triassic and associated rocks of the Naxhlak and Aghdarband areas in central and northeastern Iran as remnants of the southern Turanian active continental margin. *Geol Soc Am Bull* 109:1563–1575
- Alesi EJ (1984) Der Trigonodus-Dolomit im Oberen Muschelkalk von SW-Deutschland. *Arb Geol Paläont Inst Univ Stuttgart N F* 79:1–53
- Al-Husseini M (1997) Jurassic sequence stratigraphy of the Western Arabian Gulf. *GeoArabia* 2:361–380
- Allen MB, Ghassemi MR, Shahabi M, Qorashi M (2003) Accommodation of late Cenozoic oblique shortening in the Alborz range, northern Iran. *J Struct Geol* 25:659–672
- Alsharhan AS, Kendall CGSTC (2003) Holocene coastal carbonates and evaporites of the southern Arabian Gulf and their ancient analogues. *Earth-Sci Rev* 61:191–243
- Alsharhan AS, Magara K (1995) Nature and distribution of porosity and permeability in Jurassic carbonate reservoirs of the Arabian Gulf Basin. *Facies* 32:37–254
- Amirshahkarami M, Vaziri-Moghaddam H, Taheri A (2007) Paleo-environmental model and sequence stratigraphy of the Asmari Formation in southwest Iran. *Hist Biol* 19:173–183
- Aurell M, Robles S, Badenas B, Rosales I, Quesada S, Melendez G, Garcia-Ramos JC (2003) Transgressive–regressive cycles and Jurassic palaeogeography of northeast Iberia. *Sediment Geol* 162:239–271
- Azeredo AC, Wright VP, Ramalho MM (2002) The Middle–Late Jurassic forced regression and disconformity in central Portugal: eustatic, tectonic and climatic effects on a carbonate ramp system. *Sedimentology* 49:1339–1370
- Bachmann M, Hirsch F (2006) Lower Cretaceous carbonate platform of the eastern Levant (Galilee and the Golan Heights): stratigraphy and second-order sea-level change. *Cret Res* 27:487–512
- Badenas B, Aurell M (2010) Facies models of a shallow-water carbonate ramp based on distribution of non-skeletal grains (Kimmeridgian, Spain). *Facies* 56:89–110
- Bassi D, Nebelsick JH (2010) Components, facies and ramps: redefining Upper Oligocene shallow-water carbonates using coralline red algae and larger foraminifera (Venetian area, northeast Italy). *Palaeogeogr Palaeoclimatol Palaeoecol* 295:258–280
- Biskaborn B (2009) The Upper Jurassic of Gräfenberg (Southern Germany): implications for microfacies development and relative sea-level change. *Berliner Paläobiol Abh* 10:49–60
- Brachert TC, Hultsch N, Knoerich AC, Krautworst UMR, Stuchkrad OM (2001) Climatic signatures in shallow-water carbonates: high resolution stratigraphic markers in structurally controlled carbonate buildups (Late Miocene, Southern Spain). *Palaeogeogr Palaeoclimatol Palaeoecol* 175:211–237
- Brigaud BFG, Vincent DC, Deconinck GF, Blanc P, Trouiller A (2010) Acoustic properties of ancient shallow marine carbonates: effect of depositional environments and diagenetic processes (Middle Jurassic, Paris Basin, France). *J Sediment Res* 80:791–807
- Brookfield ME, Hashmat A (2001) The geology and petroleum potential of the North Afghan platform and adjacent areas (northern Afghanistan, with parts of southern Turkmenistan, Uzbekistan and Tajikistan). *Earth-Sci Rev* 55:41–71
- Brunet MF, Korotaev MV, Ershov AV, Nikishin AM (2003a) The South Caspian Basin: a review of its evolution from subsidence modelling. *Sediment Geol* 156:119–148
- Brunet MF, Korotaev MV, Ershov AV, Nikishin AM (2003b) The South Caspian Basin: a review of its evolution from subsidence modeling. *Sediment Geol* 156:119–148
- Brunet MF, Wilmsen M, Granath JW (eds) (2009) South Caspian to Central Iran Basins. *Geol Soc Lond Spec Publ* 312, 360 p
- Buckovic D, Delaska V, Cvetko TB (2001) Facies variability in Lower Liassic carbonate successions of the western Dinarides (Croatia). *Facies* 44:151–162
- Buonocunto FP, D’Argenio B, Ferreri V, Raspini A (1994) Micro-stratigraphy of highly organized carbonate platform deposits of Cretaceous age. The case of Serra Sbragavitelli, Matese (Central Apennines). *Giorn Geol* 56:179–192
- Burchette TP, Wright VP (1992) Carbonate ramp depositional systems. *Sediment Geol* 79:3–57
- Carozzi AV (1993) Sedimentary petrology. Prentice Hall, Englewood Cliffs 263 p
- Catuneanu O (2006) Principles of sequence stratigraphy. Elsevier, Amsterdam 375 p
- Catuneanu O, Elango HN (2001) Tectonic control on fluvial styles: the Balfour Formation of the Karoo Basin, South Africa. *Sediment Geol* 140:291–313
- Catuneanu O, Abreu V, Bhattacharya JP, Blum MD, Dalrymple RW, Eriksson PG, Fielding CR, Fisher WL, Galloway WE, Gibling MR, Giles KA, Holbrook JM, Jordan R, Kendall CGSTC, Macurda B, Martinsen OJ, Miall AD, Neal JE, Nummedal D, Pomar L, Posamentier HW, Pratt BR, Sarg JF, Shanley KW, Steel RJ, Strasser A, Tucker ME, Winker C (2009) Towards the standardization of sequence stratigraphy. *Earth-Sci Rev* 92:1–33
- Claps M, Trombetta GL, Picotti V (1996) Il bioerma del M. Zenone (Norico, Prealpi Bresciane): facies, geometria e ambiente deposizionale. *Atti Tic Sci Terra Spec Ser* 4:3–18
- Clarke JW (1994) Petroleum potential of the Amu-Dar’ya Province, western Uzbekistan and eastern Turkmenistan. *Int Geol Rev* 36:407–415
- Corda L, Brandano M (2003) Aphotic zone carbonate production on a Miocene ramp, Central Apennines, Italy. *Sediment Geol* 61:55–70
- Cortes JE, Gomez JJ, Goy A (2009) Facies associations, sequence stratigraphy and timing of the earliest Jurassic peak transgression in central Spain (Iberian Range): correlation with other Lower Jurassic sections. *J Iber Geol* 35:47–58
- Cosovic V, Drobne K, Moro A (2004) Paleoenvironmental model for Eocene foraminiferal limestones of the Adriatic carbonate platform (Istrian Peninsula). *Facies* 50:61–75

- Cozzi Z (2002) Facies patterns of a tectonically-controlled Upper Triassic platform-slope carbonate depositional system (Carnian Prealps, Northeastern Italy). *Facies* 47:151–178
- Davies SJ, Gibling MR (2003) Architecture of coastal and alluvial deposits in an extensional basin: the Carboniferous Joggins Formation of eastern Canada. *Sedimentology* 50:415–439
- Davoudzadeh M, Schmidt K (1981) Contribution to the paleogeography of the Upper Triassic to Middle Jurassic of Iran. *N J Geol Paläont Abh* 162:137–163
- Decarlis A, Lualdi A (2009) A sequence stratigraphic approach to a Middle Triassic shelf-slope complex of the Ligurian Alps (Ligurian Briançonnais, Monte Carmo-Rialto unit, Italy). *Facies* 55:267–290
- Demirtasli E (1984a) Stratigraphic evidence of Variscan and early Alpine tectonics in southern Turkey. In: Dixon JE, Robertson AHF (eds) *The Geological evolution of the eastern Mediterranean*. *Geol Soc Lond Spec Publ* 17:129–146
- Demirtasli E (1984b) Stratigraphy and tectonics of the area between Silifke and Anamur, Central Taurus Mountains. In: Tekeli O, Göncüoğlu MC (eds) *Geology of the Taurus Belt*. *Proc Int Tauride Symp. Min Res and Explor Inst of Turkey (MTA) Publ*, pp 101–118
- Dercourt J, Gaetani M, Vrielynck B, Barrier E, Bijou-Duval B, Brunet MF, Cadet JP, Crasquin S, Sandulescu M (eds) (2000) *Atlas Peri-Tethys, Palaeogeographical Maps*. CCGM/CGMW, Paris, 268 p
- Dickson JAD (1966) Carbonate identification and genesis as revealed by staining. *J Sediment Petrol* 36:441–505
- Dunham RJ (1962) Classification of carbonate rocks according to depositional textures. In: Ham WE (ed) *Classification of carbonate rocks*. *Am Assoc Petrol Geol Mem* 1:108–121
- Embry AF, Klovan JE (1971) A late Devonian reef tract on northeastern Banks Island, Northwest Territories. *Bull Can Petrol Geol* 19:730–781
- Flügel F (2010) *Microfacies of carbonate rocks—analysis, interpretation and application*. Springer, Berlin Heidelberg New York
- Folk RL (1962) Spectral subdivision of limestone types. In: Ham WE (ed) *Classification of carbonate rocks*. *Am Assoc Petrol Geol Mem* 1:62–84
- Fürsich FT, Wilmsen M, Seyed-Emami K, Schairer G, Majidifard MR (2003) Platform-basin transect of a Middle to Late Jurassic large-scale carbonate platform system (Shotori Mountains, Tabas Area, East-Central Iran). *Facies* 48:171–198
- Fürsich FT, Wilmsen M, Seyed-Emami K, Cecca F, Majidifard MR (2005) The upper Shemshak Formation (Toarcian-Aalenian) of the Eastern Alborz (Iran): biota and palaeoenvironments during a transgressive–regressive cycle. *Facies* 51:365–384
- Fürsich FT, Wilmsen M, Seyed-Emami K, Majidifard MR (2009) The Mid-Cimmerian tectonic event (Bajocian) in the Alborz Mountains, northern Iran: evidence of the break-up unconformity of the South Caspian Basin. In: Brunet MF, Wilmsen M, Granath J (eds) *South Caspian to Central Iran basins*. *Geol Soc Lond Spec Publ* 312:189–203
- Geel T (2000) Recognition of stratigraphic sequences in carbonate platform and slope deposits: empirical models based on microfacies analysis of Paleogene deposits in southeastern Spain. *Paleogeogr Paleoclimatol Paleocool* 155:211–238
- Ghasemi-Nejad E, Sabbaghian H, Mosaddegh H (2012) Palaeobiogeographic implications of Late Bajocian–Late Callovian (Middle Jurassic) dinoflagellate cysts from the Central Alborz Mountains, northern Iran. *J Asian Earth Sci* 43:1–10
- Golonka J (2004) Plate tectonic evolution of the southern margin of Eurasia in the Mesozoic and Cenozoic. *Tectonophysics* 381:235–273
- Hallam A (2001) A review of the broad pattern of Jurassic sea-level changes and their possible causes in the light of current knowledge. *Palaeogeogr Palaeoclimatol Palaeocool* 167:23–37
- Haq BU, Hardenbol J, Vail PR (1988) Mesozoic and Cenozoic chronostratigraphy and cycles of sea-level change. In: Wilgus CK, Hastings BS, Kendall CGStC, Posamentier HW, Ross CA, Van Wagoner JC (eds) *Sea-level changes—an integrated approach*. *SEPM Spec Publ* 42:71–108
- Herrmann R (1996) Entwicklung einer oberjurassischen Karbonatplattform: biofazies, Riffe und Sedimentologie im Oxfordium der Zentralen Dobrogea (Ost-Rumänien). *Berliner Geowiss Abh E* 19:1–101
- Hips K, Haas J (2009) Facies and diagenetic evaluation of the Permian–Triassic boundary interval and basal Triassic carbonates: shallow and deep ramp sections, Hungary. *Facies* 55:421–442
- Hips K, Pelikan P (2002) Lower Triassic shallow marine succession in the Bükk Mountains, NE Hungary. *Geol Carpath* 53:351–367
- Husinec A, Sokac B (2006) Early Cretaceous benthic associations (foraminifera and calcareous algae) of a shallow tropical-water platform environment (Mljet Island, southern Croatia). *Cret Res* 27:418–441
- Jacquin T, Dardeau G, Durllet C, Gracianski PC, Hantzpergue P (1998) The North sea cycle: an overview of 2nd-order transgressive/regressive facies cycles in Western Europe. In: de Gracianski PC, Hardenbol J, Jacquin T, Vail PR (eds) *Mesozoic and Cenozoic sequence stratigraphy of European basins*. *SEPM Spec Publ* 60:445–466
- James NP, Bone Y, Collins LB, Kyser TK (2001) Surficial sediments of the Great Australian Bight: facies dynamics and oceanography on a vast cool-water carbonate shelf. *J Sediment Res* 71:549–567
- Jank M, Wetzel A, Meyer C (2006) Late Jurassic sea-level fluctuations in NW Switzerland (Late Oxfordian to Late Kimmeridgian): closing the gap between the Boreal and Tethyan realm in Western Europe. *Facies* 52:487–519
- Kavoosi MA, Lasemi Y, Sherkati S, Moussavi-Harami R (2009) Facies analysis and depositional sequences of the Upper Jurassic Mozduran Formation, a carbonate reservoir in the Kopet Dag Basin, NE Iran. *J Petrol Geol* 32:235–260
- Kazmin VG (1989) Collision and rifting history of the Tethys Ocean. *Geotectonics* 23:391–399
- Lasemi Y (1995) Platform carbonates of the Upper Jurassic Mozduran Formation in the Koppeh Dag Basin, NE Iran: facies, paleoenvironments and sequences. *Sediment Geol* 99:151–164
- Mahboubi A, Moussavi-Harami R, Aghaei A, Aletaha H (2006) Sequence stratigraphy and palaeogeography of the Upper Jurassic reservoir equivalent along the outcrop belt in the Agh-Darband area, northeastern Iran. In: 6th International conference on the geology of the Middle East, Al-Ain, United Arab Emirates, pp 20–23
- Mahboubi A, Moussavi-Harami R, Aghaei A, Carpenter SJ, Collins LB (2010) Petrographical and geochemical evidences for paragenetic sequence interpretation of diagenesis in mixed siliciclastic–carbonate sediments: Mozduran Formation (Upper Jurassic), south of Agh-Darband area, NE Iran. *Carb Evap* 25:231–246
- Majidifard MR (2008) Stratigraphy and facies analysis of the Dalichai and Lar formations (Middle-Upper Jurassic) of NNE Iran. *Beringeria* 39:3–49
- Martini R, Cirilli S, Saure C, Abate B, Ferruzza G, Cicero GL (2007) Depositional environment and biofacies characterisation of the Triassic (Carnian to Rhaetian) carbonate succession of Punta Bassano (Marettimo Island, Sicily). *Facies* 53:389–400
- Matyszkiewicz J, Krajewski M, Tyc A, Krol K, Kedziński J, Jedryś J, Świader J (2004) Facial development of the Upper Jurassic complex of the Zegarowe Rocks near Smolen (Kraków-Wielun Upland; southern Poland) In: Partyka J (ed) *Zróznicowanie i przemiany środowiska przyrodniczo-kulturowego Wyżyny*

- Krakowsko-Czestochowskiej. Ojcowski Park Narodowy 1:35–42 (with English abstract)
- Moix P, Beccalotto L, Kozur HW, Hochard C, Rosselet F, Stampfli GM (2008) A new classification of the Turkish terranes and sutures and its implication for the paleotectonic history of the region. *Tectonophysics* 451:7–39
- Moosavirad SM, Janardhan MR, Sethumadhav MS, Moghadam MR, Shankara M (2011) Geochemistry of lower Jurassic shales of the Shemshak Formation, Kerman Province, Central Iran: Provenance, source weathering and tectonic setting. *Chemie der Erde Geochem* 71:279–288
- Nalin R, Nelson CS, Basso D, Massari F (2008) Rhodolith-bearing limestones as transgressive marker beds: fossil and modern examples from North Island, New Zealand. *Sedimentology* 55:249–274
- Palma RM, Lopez-Gomez J, Piethe RD (2007) Oxfordian ramp system (La Manga Formation) in the Bardas Blancas area (Mendoza Province) Neuquen Basin, Argentina: facies and depositional sequences. *Sediment Geol* 195:113–134
- Papaioannou FP, Kostopoulou V (2008) Microfacies and cycle stacking pattern in Liassic peritidal carbonate platform strata, Gavrovo-Tripolitza platform, Peloponnesus, Greece. *Facies* 54:417–443
- Pedley HM, Carannante G (2006) Cool-water carbonate ramps: a review. In: Pedley HM, Carannante G (eds), *Cool-water carbonates: depositional systems and palaeoenvironmental controls*. *Geol Soc Lond Spec Publ* 255:1–9
- Pomar L (2001a) Types of carbonate platforms: a genetic approach. *Basin Res* 13:313–334
- Pomar L (2001b) Ecological control of sedimentary accommodation: evolution from a carbonate ramp to rimmed shelf, Upper Miocene, Balearic Islands. *Paleogeogr Paleoclimatol Paleocol* 175:249–272
- Ramezani Oomali R, Shahriari S, Hafezi Moghadams N, Omidi P, Eftekharijeh J (2008) A model for active tectonics in Kopet Dagh (North-East Iran). *World Appl Sci J* 3:312–316
- Ritz JF, Nazari H, Ghassemi A, Salamati R, Shafei A, Solaymani S, Vernant P (2006) Active transtension inside central Alborz: a new insight into northern Iran–southern Caspian geodynamics. *Geology* 34:477–480
- Romero J, Caus E, Rossel J (2002) A model for the palaeoenvironmental distribution of larger foraminifera based on Late Middle Eocene deposits on the margin of the south Pyrenean Basin (SE Spain). *Paleogeogr Paleoclimatol Paleocol* 179:43–56
- Ruf M, Link E, Pross J, Aigner T (2005) A multi-proxy study of deeper-water carbonates (Upper Jurassic, southern Germany): combining sedimentology, chemostratigraphy and palynofacies. *Facies* 51:326–349
- Rush J, Kerans C (2010) Stratigraphic response across a structurally dynamic shelf: the latest Guadalupian Composite sequence at Walnut Canyon, New Mexico, USA. *J Sediment Res* 80:808–828
- Schauer M, Tebingen TA (1997) Cycle stacking pattern, diagenesis and reservoir geology of peritidal dolostones, Trigonodus-Dolomit, Upper Muschelkalk (Middle Triassic, SW Germany). *Facies* 37:99–114
- Schlager W (2005) Sedimentology and sequence stratigraphy of carbonate rocks. *Concepts Sediment Paleont* 8:1–200
- Schlagintweit F, Gawlick HJ (2009) Oncoïd-dwelling foraminifera from Late Jurassic shallow-water carbonates of the Northern Calcareous Alps (Austria and Germany). *Facies* 55:259–266
- Sengör AMC (1979) Mid-Mesozoic closure of Permo-Triassic Tethys and its implications. *Nature* 279:590–593
- Sengör AMC (1990) A new model for the late Palaeozoic–Mesozoic tectonic evolution of Iran and implications on Oman. In: Robertson AHF, Searle MP (eds) *The geology and tectonics of the Oman region*. *Geol Soc Lond Spec Publ* 49:797–834
- Seyed-Emami K (2003) Triassic in Iran. *Facies* 48:91–106
- Seyed-Emami K, Schairer G (2011) Late Jurassic (Oxfordian, Bifurcatus and Bimammatum zones) ammonites from the eastern Alborz Mountains, Iran; second part. *N J Geol Paläont Abh* 260:11–20
- Seyed-Emami K, Fürsich FT, Wilmsen M (2004) Documentation and significance of tectonic events in the northern Tabas Block (east-central Iran) during the Middle and Late Jurassic. *Riv Ital Paleont Stratigr* 110(1):163–171
- Seyed-Emami K, Fürsich FT, Wilmsen M, Majidifard MR, Shekarifard A (2008) Jurassic ammonite fauna of the Shemshak Formation at Shahmirzad, Iran. *Acta Palaeont Polon* 53:237–260
- Shabaniyan E, Bellier O, Abbassi MR, Siame L, Farbod Y (2010) Plio-Quaternary stress states in NE Iran: Kopet Dagh and Allah Dagh-Binalud mountain ranges. *Tectonophysics* 480:280–304
- Shams M (2007) Stratigraphy and palaeontology of the Dalichai Formation in Parvar area, north of Semnan, Central Alborz, based on ammonites. Unpubl MSc Thesis, University of Teheran, Teheran, 264 p (in Farsi)
- Spengler AE, Read JF (2010) Sequence development on a sediment-starved, low accommodation epeiric carbonate ramp: Silurian Wabash Platform, USA mid-continent during icehouse to greenhouse transition. *Sediment Geol* 224:84–115
- Stampfli GM, Borel GD (2002) A plate tectonic model for the Paleozoic and Mesozoic constrained by dynamic plate boundaries and restored synthetic oceanic isochrons. *Earth Planet Sci Lett* 196:17–33
- Stampfli G, Marcoux J, Baud A (1991) Tethyan margins in space and time. *Paleogeogr Paleoclimatol Paleocol* 87:373–409
- Steiger T, Cousin M (1984) Microfacies of the Late Jurassic to Early Cretaceous carbonate platform at the Mazagan escarpment (Morocco). *Oceanol Acta* 7:111–126
- Strasser A (1986) Ooids in Purbeck limestones (Lowermost Cretaceous) of the Swiss and French Jura. *Sedimentology* 33:711–727
- Taylor SP, Sellwood BW, Gallois RW, Chambers MH (2001) A sequence stratigraphy of the Kimmeridgian and Bolonian stages (Late Jurassic): Wessex–Weald Basin, southern England. *J Geol Soc Lond* 158:179–192
- Thierry J (2000) Middle Callovian (157–155 Ma). In: Dercourt J, Gaetani M, Vrielynck B, Barrier E, Biju-Duval B, Brunet MF, Cadet JP, Crasquin S, Sandulescu M (eds) *Atlas Peri-Tethys, Palaeogeographical Maps*. CCGM/CGMW, Paris, pp 1–97
- Thomas JC, Cobbold PR, Shein VS, Douaran SL (1999) Sedimentary record of late Paleozoic to Recent tectonism in central Asia—analysis of subsurface data from the Turan and south Kazak domains. *Tectonophysics* 313:243–263
- Tucker ME, Wright VP (1990) *Carbonate sedimentology*. Blackwell, Oxford 482 p
- Van Buchem FSP, Gerdes KD, Esteban M (2010) Mesozoic and Cenozoic carbonate systems of the Mediterranean and the Middle East: stratigraphic and diagenetic reference models. *Geol Soc Lond Spec Publ* 329:1–7
- Van Wagoner JC, Posamentier HW, Mitchum RM, Vail PR, Sarg JF, Loutit TS, Hardenbol J (1988) An overview of sequence stratigraphy and key definitions. In: Wilgus, CK, Hastings BS, Kendall CGStC, Posamentier HW, Ross CA, Van Wagoner JC (eds) *Sea level changes—an integrated approach*. *Soc Econ Paleont Miner Spec Publ* 42:39–45
- Van Wagoner JC, Mitchum JRM, Campion KM, Rahmanian VD (1990) Siliciclastic sequence stratigraphy in well logs, core, and outcrops: concepts for high-resolution correlation of time and facies. *Am Assoc Petrol Geol Meth Explor Ser* 7:55
- Vaziri-Moghaddam H, Kimiagari M, Taheri A (2006) Depositional environment and sequence stratigraphy of the Oligo-Miocene Asmari Formation in SW Iran. *Facies* 52:41–51

- Wignall PB (1994) *Black Shales*. Oxford University Press, Oxford 136 p
- Wilmsen M, Fürsich FT, Seyed-Emami K (2003) Revised lithostratigraphy of the Middle and Upper Jurassic Magu Group of the northern Tabas Block, east-central Iran. *Newsl Stratigr* 39:143–156
- Wilmsen M, Fürsich FT, Seyed-Emami K, Majidifard MR, Taheri J (2009a) The Cimmerian Orogeny in northern Iran: tectono-stratigraphic evidence from the foreland. *Terra Nova* 21:211–218
- Wilmsen M, Fürsich FT, Seyed-Emami K, Majidifard MR (2009b) An overview of the lithostratigraphy and facies development of the Jurassic System on the Tabas Block, east-central Iran. In: Brunet MF, Wilmsen M, Granath J (eds) *South Caspian to central Iran basins*. *Geol Soc Lond Spec Publ* 312:323–344
- Wilmsen M, Fürsich FT, Seyed-Emami K, Majidifard MR, Zamani PM (2010) Facies analysis of a large-scale Jurassic shelf-lagoon: the Kamar-e-Mehdi Formation of east-central Iran. *Facies* 56:59–87
- Wilson JL (1975) *Carbonate facies in geologic history*. Springer, Berlin Heidelberg New York
- Wilson MEJ, Evans MEJ (2002) Sedimentology and diagenesis of Tertiary carbonates on the Mangkalihat Peninsula, Borneo: implications for subsurface reservoir quality. *Mar Petrol Geol* 19:873–900
- Wright VP, Burchette TP (eds) (1998) *Carbonate ramps*. *Geol Soc Lond Spec Publ* 149:1–462
- Zagrarni MF, Negra MH, Hanini A (2008) Cenomanian–Turonian facies and sequence stratigraphy, Bahloul Formation, Tunisia. *Sediment Geol* 204:18–35
- Zanchi A, Berra F, Mattei M, Ghassemi MR, Sabouri J (2006) Inversion tectonics in central Alborz, Iran. *J Struct Geol* 28:2023–2037
- Zonenshain LP, Le Pichon X (1986) Deep basins of the Black Sea and Caspian Sea as remnants of Mesozoic back-arc basins. *Tectonophysics* 123:181–211